Numerical analysis of pipeline uplift resistance in a frozen clay soil subjected to temperature changes

Sohail Akhtar

A Thesis

In

The Department

Of

Building, Civil, and Environmental Engineering

Presented in Partial Fulfillment of the Requirements

For the Degree of

Master of Applied Science (Geotechnical Engineering) at

Concordia University

Montréal, Québec, Canada

November 2018

CONCORDIA UNIVERSITY

School of Graduate Studies

This is to certify that the thesis prepared

By: **Sohail Akhtar**

Entitled: **Numerical analysis of pipeline uplift resistance in a frozen clay soil subjected to temperature changes**

and submitted in partial fulfillment of the requirements for the degree of

Master of Applied Science (Geotechnical Engineering)

complies with the regulations of the University and meets the accepted standards with respect to originality and quality.

Signed by the final Examining Committee:

Chair and Examiner

Dr. Adel M. Hanna

Examiner

Dr. Yong Zeng

Examiner

Dr. Attila Michael Zsaki

Supervisor

Dr. Biao Li

Approved by: Chair of the Department or Graduate Program Director

Dean of Faculty

Date:

ABSTRACT

Frozen clay soils comprise a large portion of permafrost in Canada. Long-term records indicate an on-going global warming has resulted in the thawing of portions of the permafrost area, which leads to extensive settlement of the ground surface and causing damage to infrastructures such as pipelines. The design of buried pipelines in permafrost region or artificially frozen grounds requires knowledge of the uplift resistance. The uplift resistance of a frozen soil is dependent on soil mechanical properties such as tensile strength, shear strength, and deformation modulus, and those properties are critical for characterizing the plastic yielding zones in the frozen soil around the pipe. Due to the existence of a large amount of unfrozen water, frozen clay soil displays complex mechanical properties which vary with temperatures. Previously, extensive experimental and simulation work has been done on the soil pipe interactions at normal temperatures, but less attention is given to the frozen soil pipe interactions. There are limited researches on frozen clay pipe interactions with the consideration of temperature changes.

In this study, the finite element analysis is conducted to investigate frozen clay soil-pipe interactions at varying temperatures, where a pipe is simulated as being subjected to vertical load-controlled or vertical displacement-controlled stress path conditions. The temperature-dependent mechanical properties of frozen clay soil are obtained from the literature. Both tensile yielding and shear yielding behavior are included in the modeling and the temperature-dependent yielding surfaces are included in an explicit way. Modeled stress paths in several soil monitoring points are collected and analyzed. A comparison of results from the Mohr-Coulomb model with tensile cut off and the hyperbolic Drucker-Prager model is presented. The results indicate that

hyperbolic Drucker-Prager model is an effective model for analyzing the plastic zones. Under a plane strain condition, the applied hyperbolic Drucker-Prager model gives more conservative uplift resistance-displacement relation when compared with the result from the Mohr-Coulomb model.

Keywords: Frozen soil, unfrozen water content, temperature dependent mechanical parameters, transient heat flow, Mohr-Coulomb failure criterion, hyperbolic Drucker-Prager failure criterion.

ACKNOWLEDGMENT

I would like thanks and sincere gratitude to Dr. Biao Li, for all his guidance, encouragement, and suggestions towards problems solving and his hard working for teaching various techniques and required software knowledge, during my master's program, which undoubtedly helps me to be determinant throughout the ups and downs of research work.

I also wish to express my sincere gratitude to Higher Education Commission, Pakistan for financial support of my higher education in Canada and giving me a chance to extend my knowledge for the betterment of both my country and ongoing research in the locality.

I would also thank the examination committee for reading this thesis and providing critical comments.

Last but by no means least, I would like to thank my family, although they were far away from me, but their love and endless psychological support kept encouraging me to persist forward during my study.

Table of Contents

LIST OF FIGURES

LIST OF TABLES

LIST OF SYMBOLS, ABBREVIATIONS AND NOMENCLATURE

c	Cohesive strength in Mohr-Coulomb criterion
C_0	Uniaxial compressive strength
d, d'	Drucker-Prager cohesion
HDP	Hyperbolic Drucker-Prager
$I_1 = \sigma_1 + \sigma_2 + \sigma_3$	First invariant of the stress tensor
$J_2 = \frac{1}{2} s_{ij} s_{ij}$	Second invariant of stress deviatoric tensor
$J_3 = \lvert s_{ij} \rvert$	Third invariant of stress deviatoric tensor
k	Yield stress in pure shear
MCR	Mohr-Coulomb with Rankine tensile cutoff
$p = -\frac{1}{3} trace(\sigma)$	Equivalent pressure stress
$P_t \vert_0$	The initial tensile strength of the material
q	Von Mises equivalent shear stress
s_{ij}	Deviatoric stress tensor
STT	Split tensile test
$\bar{\sigma}$	Equivalent stress deviatoric tensor
β	Drucker-Prager friction angle

ε^{pl}	Equivalent plastic strain
ϵ	Eccentricity parameter defines the rate at which the function approaches the asymptote
ϕ, ϕ_{max}	Friction angle in Mohr-Coulomb criterion
ϕ_{cri}	Friction angle in a critical state or residual friction angle
ψ	Dilation angle
$\rho = \sqrt{2J_2}$	Deviatoric length
$\sigma_1, \sigma_2, \sigma_3$	Principal stresses
$\sigma_1', \sigma_2', \sigma_3'$	Principal deviatoric stress
τ	Shear stress
$\tau_{oct} = \sqrt{\frac{2}{3} J_2}$	Octahedral shear stress
$\theta\,(\Theta)$	The angle of similarity, Lodi angle
$\xi = \frac{1}{\sqrt{3}} I_1$	Hydrostatic length
μ	Poisson's ratio

CHAPTER 1

INTRODUCTION

1.1 Background of buried pipes in frozen grounds

The transportation of natural resources (e.g. oil, gases) through pipelines are safe and economical. Pipelines are buried below the ground to avoid failure because of the external loads and harsh environmental impact on their stability. Pipelines may be buried at shallow depth or deep down depending on the carrying materials and the safety requirements. Failure of an oil and gas pipeline not only causes serious economic and environmental consequences, but it may also lead to gas explosions resulting in loss of human lives. Detailed statistical data on pipeline rupture causes is given by pipeline and hazardous material safety administration (PHMSA, 2018) and National Energy Board (NEB, 2011) as is shown in Figure 1.1.

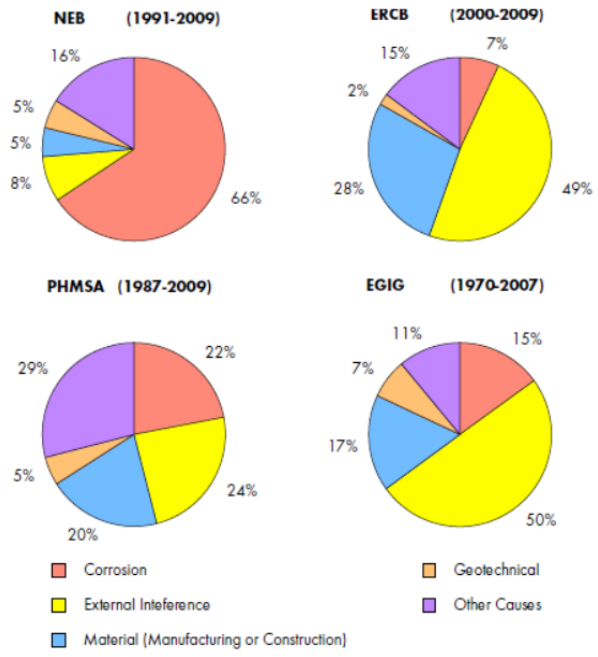

Figure 1. 1 Pie chart representing the reasons behind the failure of pipes, after NEB (2011).

Global warming results in the thawing of portions of the permafrost area, which leads to extensive settlement of the ground surface and causing damage to infrastructures such as pipelines (Figures 1.2 and 1.3). This is due to the non-uniform initial freezing state of the soil. A reliable prediction of frozen soil uplift resistance is critical for designing the pipe profile and burial depth and is essential for facilitating life-cycle cost optimization for pipeline maintenance. Detail statistical failure data for pipelines distribution in cold weather region arranged by PHMSA (Figure 1.4), emphasizing the importance of frost heave among other reasons.

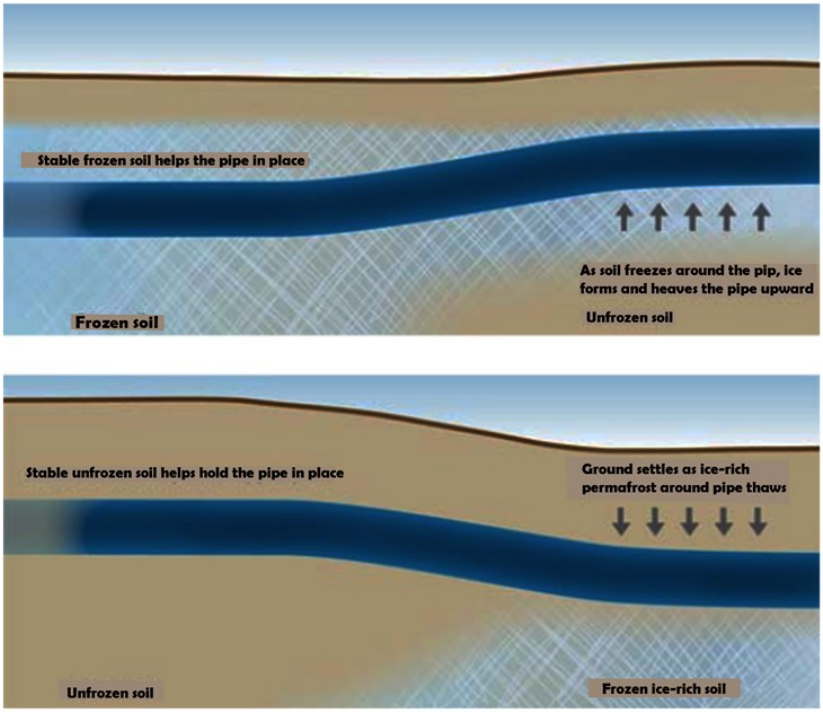

Figure 1. 2 Frost-heaving effects because of soil freezing and thawing effects because of gravity loading from settling ice-rich soils, after NEB (2012).

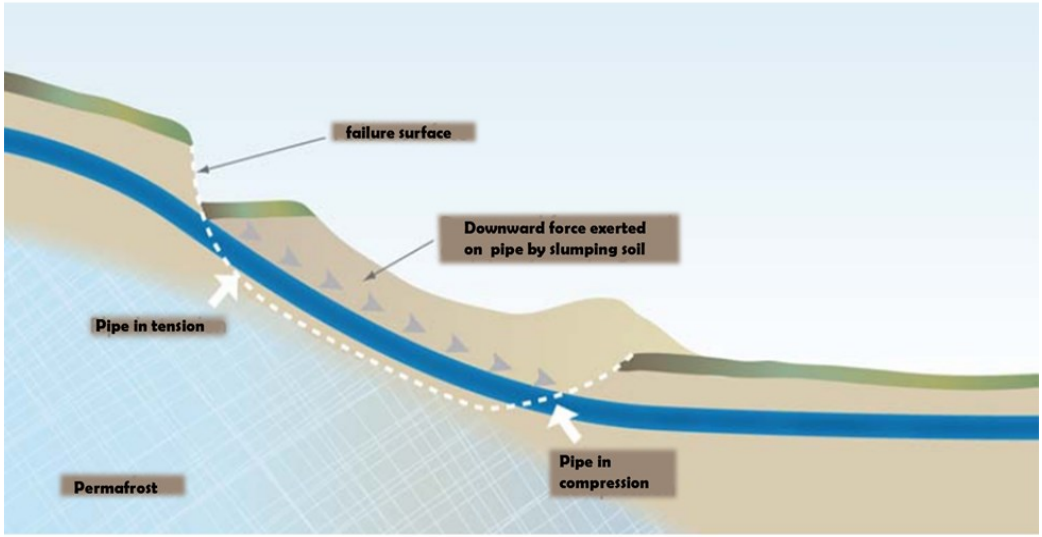

Figure 1. 3 Permanent ground deformation due to global warming which leads to long-term large strains in pipes, after NEB (2012).

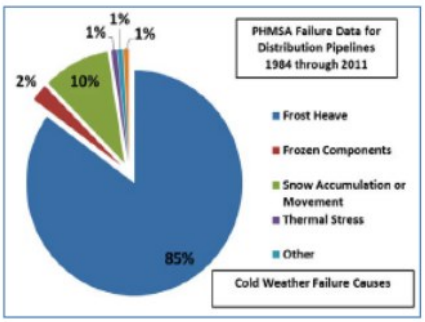

(a) Causes of pipeline in cold weather

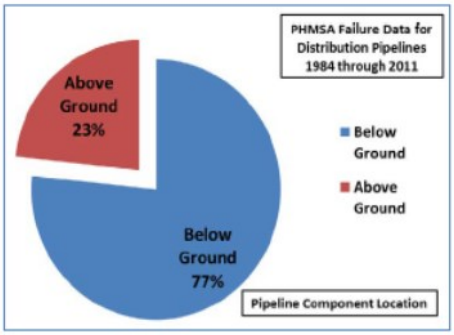

(b) Location-based failures in cold weather pipeline

Figure 1. 4 Pie chart representing the reasons behind the failure of pipelines in cold regions, after Rosenfeld and Auker (2012).

Previous researches have been conducted to investigate the physical processes of frozen soil pipeline interactions. Foriero and Ladanyi (1994) presented the numerical modeling and theoretical analytical approach as a continuation of research work done by Nixon (1984-93) for the frozen soil pipe interaction considering the soil as a continuum matrix. Pipe uplift resistance in the frozen soil was studied to monitor a gradual pipe heave near an interface between two soils of different heave potentials. Tensile cracks and compression fracture zones were also identified. But for the sake of simplicity, they did not consider the temperature-dependent complex behavior of frozen soils. This intuitive approach was concluded at a fixed temperature and does not consider the near field of soil to pipe cracking, which still plays an important role in real field cases.

Razaqpur and Wang (1996) treated the soil as uniform spring and the pipe as an elastic beam, which is the simplified approach of studying frozen soil pipe interaction. But the study did

not include the field conditions where soil pipe interface plays an important role during loading condition and ignored the temperature-dependent mechanical properties of soil.

Nixon (1998) presented the impact of long-term strains produced at frozen-unfrozen interfaces in frost heaving terrain. The increase of uplift displacement of pipe leads to tensile crack at the vertical surface of the soil which propagates inside toward pipe and a tensile crack radiated from both horizontal sides of the pipe.

The experimental work performed by Liu et al. (2004a) and numerical model analyses performed in Liu et al. (2004b) concluded that the tensile failures radiated at the vertical top of pipeline and the spring lines of pipe followed by shear cracks because of soil mass compression due to the uplift displacement of pipe as shown in Figure 1.5 and Figure 1.6. But the frozen soil under consideration was analyzed at a single frozen temperature studying the thawing and frost heave effects on the pipeline.

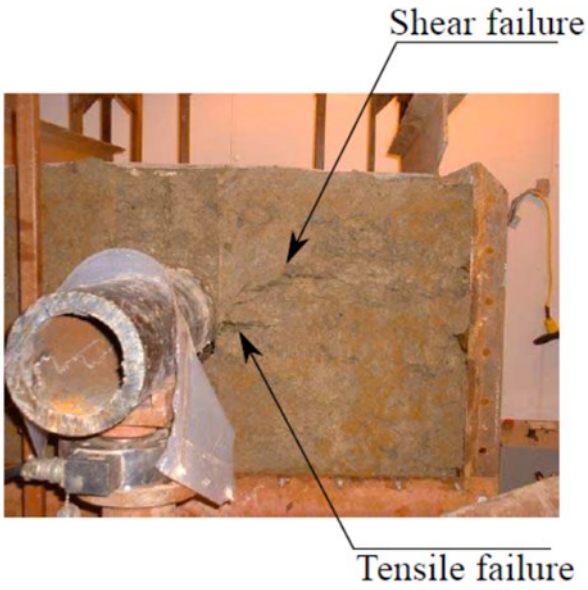

Figure 1. 5 Tensile and shear fractures observed in the uplift tests on soil-pipe interaction, after Liu et al. (2004a).

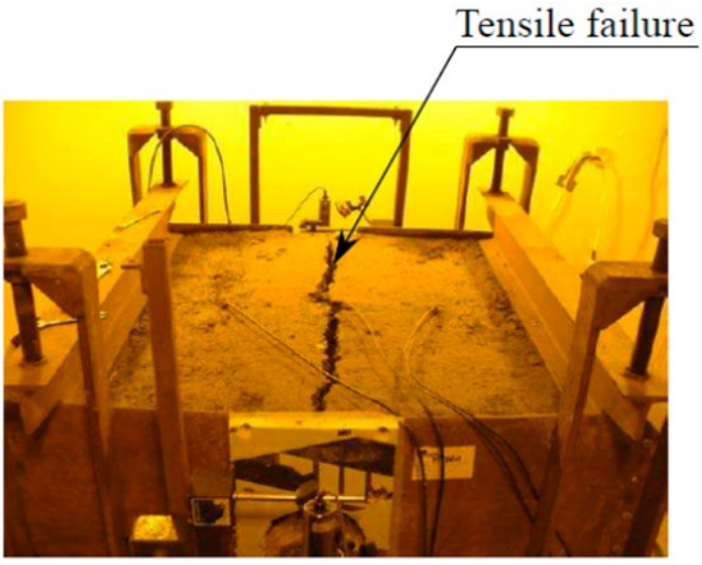

Figure 1. 6 Tensile fractures on the top part of a frozen soil matrix observed in the uplift tests on soil-pipe interaction, after Liu et al. (2004a).

From previous experimental work, we noticed the importance of considering tensile and shear failure behavior in uplift resistance analysis of buried pipes in frozen soil. However, such a hybrid failure mode was not considered in previous numerical modeling. In addition, most previous studies only focus on soil pipe interactions at constant temperatures, and little attention is given to the frozen soil pipe interactions at varying temperatures. Due to the existence of a large amount of unfrozen water, frozen clay soil displays complex mechanical properties which vary with temperatures. There are limited researches on frozen clay-pipe interactions with the consideration of temperature changes.

1.2 Objectives

1) To investigate the temperature-dependent mechanical properties of frozen silty clay soils.

2) Propose an approach for modeling pipeline uplift resistance in frozen clay with the consideration of tensile and shear yielding behaviors.

3) Perform finite element analysis on pipeline resistance in frozen clay at temperature changing conditions.

1.3 Organization of the thesis

This thesis is divided into five chapters. The first chapter gives the introduction with emphasis on the significance and objectives of this research.

Chapter 2 includes the literature reviews of the temperature-dependent mechanical strength parameters of frozen soil and the review of complex behavior (non-linear to linear response) of the warm frozen soil. Causes of permanent soil deformation and its effects on the

soil-pipe interaction in both room temperature and in the frozen stage are also presented. The determination of the expected tensile and shear zone in the monitoring points during pipe uplift movement from previous researchers is reported. Progressive developments and limitations in previous studies during the investigation of frozen-soil pipe interactions are presented, which lays the foundation for studying the impact of thermal induction on the temperature-dependent mechanical strength of frozen soil during the uplift of a pipe.

Chapter 3 presents constitutive models for the numerical analysis of frozen soil pipe interactions during uplift displacement of the pipe. The Mohr-Coulomb model with Rankine tensile cut-off (MCR) and hyperbolic Drucker-Prager (HDP) models are discussed in detail. Equations are drawn for the proper conversion of parameters from the Mohr-Coulomb model to Hyperbolic Drucker-Prager model in the plane strain condition. Temperature-dependent mechanical parameters are also presented, which is required in the thermal-mechanical analysis.

Chapter 4 includes the investigation and analyses of outcomes from the finite element-based software, Abaqus. The bearing capacity of a frozen clay soil under the pipe uplift condition is firstly investigated at constant frozen temperatures using a displacement-controlled approach. The frozen soil pipe interaction is also investigated using the thermal-mechanical coupled technique by the induction of heat in a system using temperature-dependent mechanical parameters for the frozen clay soil. Failure pattern is analyzed in both $p-q$ and principal stresses plane to thoroughly understand the response of frozen clay and warm-frozen clay towards pipe uplifting. The introduction and location of plastic strains in the frozen soil matrix and its propagation behavior are also investigated. A comparison study of results from using MCR models and HDP models is analyzed and presented.

Chapter 5 includes the summary, conclusion for this work and provides future recommendations for future research works.

CHAPTER 2

LITERATURE REVIEW

The stability and safety of buried pipelines are always the concerns of researchers and engineers. The yielding or failures developed in the surrounding soil during the service life of pipe can be due to freezing and thawing behavior, liquefaction in granular soils, or fault activities, which may compromise the stability of buried pipes. This chapter will present a review of previous studies on soil-pipe interaction with the highlight on frozen ground engineering.

2.1 Soil-pipe interaction

Large strains in pipelines and failures in terms of pipe cracking and buckling can be induced because of surrounding soil settlement or heave Kouretzis et al. (2014) or surface fault deformation, liquefaction-induced soil movements, and landslides Yoshikzaki et al. (2004). Problematic areas may also include loose sand deposits that are susceptible to dynamic densification which may cause permanent ground deformation Kohji and Seed (1986). Chan and Wong (2004) proposed an analytical solution for steel pipelines interacted with elasto-plastic soil in a moving slope and identified that soil movement may be because of non-uniform soil yielding and creeping.

The permanent ground deformation types depend on the pipeline's orientation with respect to the direction of the unstable soil mass movement. Longitudinal ground movements occur when the unstable soil mass moves parallel to the pipe axis. Transverse ground movements occur when the unstable soil mass moves orthogonality to the pipe axis. Deep-seated movements

are a combination of longitudinal and transverse ground movements. Transverse ground movements can be further subdivided into horizontal transverse and vertical uplift (in-plane), oblique transverse (out-of-plane) and vertical bearing ground movements Wong et al. (2016). Chan and Wong (2004) confirmed that the transverse movement has a more adverse effect on the structural stability and safety of the pipeline as compared to the longitudinal in-plane soil movements.

As cited in Hikooei (2013), Audeibert and Nayman (1977) used an analytical approach to determine the load and displacement relation by validating it with laboratory experimental data. Nyman (1984) studied the movement of pipe in the cohesionless soil where angle and direction of pipelines vary from 0 degrees for vertical uplift to 90 degrees for horizontal lateral directions. He potentially used the analogy between buried inclined anchor plates and pipelines subjected to out-of-plane (lateral-uplift) direction (Figure 2.1). The work of Nyman (1984) concluded it is always conservative to use lower bound soil strength parameters to compute soil resistance and upper bound (larger) values for yield displacements. Lateral ground movements effects were studied by O'Rourke and Trautmann (1985) to investigate the influence of depth, diameter and roughness of the pipe with respect to overlying soil mass. (Guo, 2005; Merifield et al., 2008) studied the pipe-soil interaction with vertical and horizontal movement of pipes where former, used the finite element method approach to produce force-displacement responses by using different ratios of pipe diameter and depth in clay while latter, using the same FEM approach for partially buried pipelines, by examining the influence of separation between the pipe and the soil for assessing the ultimate resistance. Jung et al. (2013) performed finite element modeling to simulate the lateral force versus displacement relationship of pipelines under 2D conditions in both dry and partially saturated sand and found the lateral force as a function of the pipe depth

and diameter representing that the later forces reached to a maximum value when the ratio of the depth of pipe to pipe diameter is in between 15-23.

Compared to the studies on soil-pipe interactions, there are very little researches on frozen soil pipe interactions. Nixon (1998) studied the vertical upward movement of pipe in frozen soil at a specific lower temperature and the findings concluded that because of the vertical displacements of pipe, two radial cracks appear at each side of pipe radiated from spring line of pipe and propagated inside the soil matrix while one tensile crack appeared at the top of soil mass and propagated towards pipe center shown in Figure 2.2. The same pattern of cracks along with shear zone identification was investigated by Liu et al. (2004a) as is discussed in chapter 1.

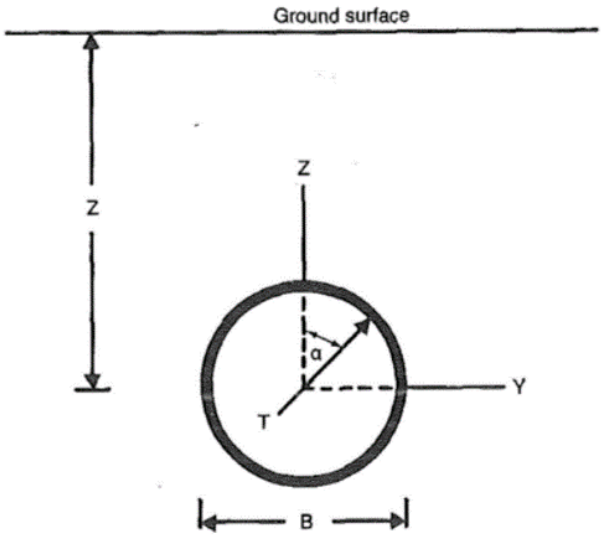

Figure 2. 1 Schematic view of Horizontal-vertical pipe movement, after Nyman (1984).

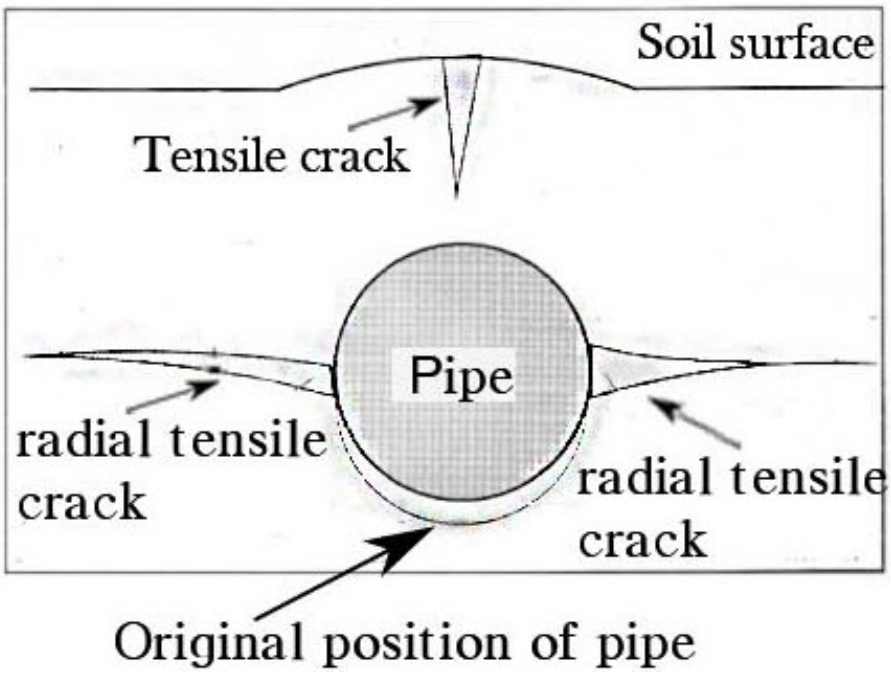

Figure 2. 2 Schematic views of pipe vertical uplift displacement in the frozen soil, after Nixon (1998).

2.2 Frozen soil strength parameters

Temperature-dependent mechanical properties play a key role in terms of stability and safety for every type of construction industry including pipelines. In the warm-frozen condition of the soil, strength parameters show a complex behavior with temperature variations. Previously, lots of researches are performed to determine the mechanical strength of soil with respect to temperature and to study the stress-strain behavior at different strain-rate conditions.

Zhao et al. (2009) determined the impact of the temperature gradient on the clay soil. They presented that the elastic modulus and compression strength increases with the decrease of

temperature and the increase of strain rate. Chen et al. (2011) presented the impact of frozen temperatures on the mechanical properties of silty clays. Their research indicates that the mechanical properties of silty clay (e.g. uniaxial compression strength, modulus of elasticity, and tensile strength) are strongly affected by the applied frozen temperatures and the strain rates. The silty clay tends to have a higher strength at a lower temperature and a higher strain rate.

The brittle effect in tensile strength along with linear relation of strength parameters with respect to temperature was identified. Azmatch et al. (2011, 2010) carried out investigation the impact of temperature, water content, and strain rate on the mechanical properties of silt. The complex behavior of warm frozen soil in terms of the non-linear relationships with the temperature determined at a temperature around – 4 ^{o}C depends on the available unfrozen water content which drastically effects the tensile strength. The influence of strain rate and freezing temperature on the silt behavior was also investigated. Leung et al. (2012) concluded the impact of lower temperature on the physical and mechanical properties of the marine deposits and alluvium soil and determined the thermal properties of the studied soil. In this study, it was determined that the specific heat capacity of the soil decreases as the temperature drops below zero degrees while thermal conductivity increases as the temperature go below zero degrees. As cited in Xu et al. (2017), there is a minor impact of confining pressure on the strength parameters and deformation characteristics of ice saturated frozen soils, and it is suggested to determine the mechanical properties of ice saturated frozen soil by uniaxial compressive test to save time and cost. Strain rate dependent mechanical strength parameters of frozen loess with respect to higher frozen temperature was analyzed. Ming et al. (2017) developed an analytical theory based on the tensile linear elastic deformation and concluded that the compressive elastic modulus gives higher values than the tensile elastic modulus using Brazilian testing technique.

2.3 Analytical and numerical analysis

Analytical and numerical analysis has been extensively applied by previous researchers to investigate soil-pipe interactions. Scarpelli et al. (2001) studied the stress induced by the slowly deforming slopes on the crossing pipelines. The pipeline was considered as elastic beam elements while the surrounding soil was modeled as mutually orthogonal 3D spring elements. Casamichele et al. (2004) carried out an analytical approach towards an impact of the seismic event while a pipe is buried in unstable slopes by assuming the ground motion perpendicular to the direction of the pipeline axis. In their research modeling, 3D soil sliding block was adopted considering infinite slope to make it close to real field case. Most of the above-mentioned researchers widely used analytical model for soil pipe interaction by means of force-displacement interactions in the lateral (p-y), vertical (q-z), axial (t-x), and oblique movement directions.

Liu et al. (2004) found a precise outcome in measurements during numerical analyses of pipe uplift resistance in frozen by comparing with a laboratory test. Their study also found the consistency in fracture initiation and propagation in numerical analyses and visual observation during laboratory experiments. Jung et al. (2013) performed finite element modeling to simulate the lateral force versus displacement relationship of pipelines under 2D, considering the soil as elastoplastic in finite element model using the Mohr-Coulomb model. Promising agreements between the large-scale laboratory test and analytical results relationship plot for lateral force were found. Rajeev and Kodikara (2011) observed the deviation of the result was less than 10 percent from experimental outcomes, their approach of numerical modeling is to give vertical upward movement of pipe in the expensive soil. Zhang and Michalowski (2015) proposed a thermal-hydro-mechanical model to study the frost heave and thaw settlement in frozen soil with

the application in footing problem. Their model was implemented in FEM. However, shear and tensile yielding of frozen soil were not considered in their numerical analysis.

2.4 Summary

The study of previous research studies is summarized as the following:

- Vertical uplift displacement of the pipe because of transition zone development in surround soil between frost heave susceptible soil and soil not susceptible to frost heave is the most critical one as compared to all transverse ground movements. The uplift movement of pipe buried in frozen soil might produce tensile fractures near both horizontal sides of pipe at mid-height and at the vertical surface of the soil.

- Strength properties, for instances, compression strength, tensile strength, modulus of elasticity and cohesion, of soil are sensitive to temperature. The decrease in temperature yields the higher values of strength parameter values. Frozen water content contributes to the cohesive strength of the soil because of its adhesion or sticking properties. The complex behavior of mechanical strength parameters of frozen soil with respect to frozen temperature gives linear trend as the temperature drops below – 4 ^{o}C, but the non-linear behavior is found, when the temperature is between – 4 ^{o}C and 0 ^{o}C.

- Numerical model analyses through the finite element or/and difference method software give close and promising results by comparing with large-scale laboratory experiments. However, the study on soil-pipe interaction with a consideration of the hybrid tensile-shear yield behavior in frozen soil is missing.

CHAPTER 3

CONSTITUTIVE MODELS FOR FROZEN CLAY SOIL

3.1 Introduction

As a key input for the numerical analysis, the constitutive model of frozen clay soil should be selected properly. In this study, we are dealing with both displacement-controlled and force-controlled behavior of the pipe buried in frozen clay soils. The applied failure criterion should be able to characterize the hybrid tensile and shear failure behavior in frozen soils. In addition, the temperature-dependent mechanical properties of frozen clay soil should be considered.

3.2 Constitutive models

Yield criterion defines the elastic limit and the starting point of plastic deformation in the material under the possible combined states of stresses. A yield criterion function can be expressed as

$$f(\sigma_{ij}, \mathrm{k}_1, \mathrm{k}_2, ...) = 0 \tag{3.1}$$

where, σ_{ij} is the stress tensor, and k_1, k_2,... are material constants. It can also be expressed in terms of principal invariant:

$$f(I_1, \mathrm{J}_2, \mathrm{J}_3, \mathrm{k}_1, \mathrm{k}_2, ...) = 0 \tag{3.2}$$

where I_1 is the first invariant of stress tensor, and J_3 are the second and the third invariants of stress deviator. In a Haigh-Westergaard coordinate, the failure function can be expressed as

$$f(\xi, \theta, \rho, k_1, k_2, ...) = 0 \tag{3.3}$$

where ξ is the hydrostatic length, θ is the angle of similarity, and ρ is the deviatoric length.

In this chapter, the following three hydrostatic pressure dependent yield criteria are given in details.

- Rankine maximum tensile stress criterion
- Mohr-Coulomb criterion
- Hyperbolic Drucker-Prager Criterion

3.2.1 Rankine maximum tensile stress yield criterion

In 1876, Rankine yield criterion was introduced, which states that when the maximum principle the stress of a point inside a brittle material equals the tensile strength σ_0 during simple tension test, brittle failure occurs while ignoring the effect of the normal or shear stresses on the point other planes. Mathematically,

$$\sigma_1 = \sigma_0, \qquad \sigma_2 = \sigma_0, \qquad \sigma_3 = \sigma_0 \tag{3.4}$$

The Rankine yield criterion has three surfaces perpendicular to the σ_1, σ_2 and σ_3 respectively. This surface is called tension cutoff or tension-failure surface. The cross-sectional

shape on the π-plane ($\xi = 0$) and the tensile ($\theta = 0^o$) and compressive ($\theta = 60^o$) meridians of failure surface is shown in Figure 3.1.

Rankine Criterion will be given by the following equations;

$$f(I_1, J_2, \theta) = 2\sqrt{3J_2}\cos\theta + I_1 - 3\sigma_0 = 0 \qquad (0 \le \theta \le 60^o) \tag{3.5}$$

Similarly,

$$f(\xi, \rho, \theta) = \sqrt{2}\rho\cos\theta + \xi - \sqrt{3}\sigma_0 = 0 \qquad (0 \le \theta \le 60^o) \tag{3.6}$$

In the documentation of Abaqus (2016), the Rankine yield function F_t is expressed as:

$$F_t = R_r(\Theta)q - p - \sigma_t(\bar{\varepsilon}_t^{pl}) = 0 \tag{3.7}$$

where $R_r(\Theta) = (2/3)\cos\Theta$; Θ is the deviatoric polar angle; p is the equivalent mean stress, q is the Mises equivalent stress; σ_t is the tensile strength, which is a function of tensile equivalent plastic strain, $\bar{\varepsilon}_t^{pl}$.

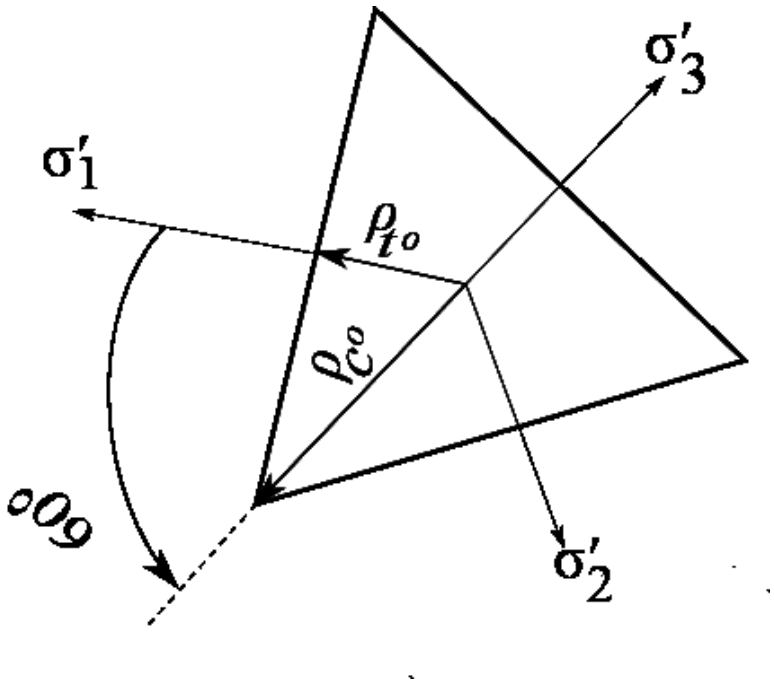

Figure 3. 1 Schematic view of the cross-section of Rankine Criteria in π-plane, after Chen and Han (1989).

A flow potential chosen for the Rankine surface is the modified version of Menetry-William potential:

$$G_t = \sqrt{(\varepsilon_t \sigma_t|_0)^2 + (R_t q)^2} - p \tag{3.8}$$

and

$$R_t(\Theta, e_t) = \frac{1}{3} \frac{4(1-e_t^2)\cos^2\Theta + (2e_t-1)^2}{2(1-e_t^2)\cos\Theta + (2e_t-1)\sqrt{4(1-e_t^2)\cos^2\Theta + 5e_t^2 - 4e_t}} \tag{3.9}$$

where e_t is the deviatoric eccentricity, and the symbol $|_0$ shows the initial values of the given parameters.

3.2.2 Mohr-Coulomb criterion

The three-dimensional failure surface of the Mohr-Coulomb criterion is expressed in Chen and Han (1989):

$$f(I_1, J_2, \theta) = \frac{1}{3} I_1 \sin\phi + \sqrt{3}\rho \sin(\theta + \frac{\pi}{3}) + \frac{\sqrt{J_2}}{3} \cos(\theta + \frac{\pi}{3}) \sin\phi - c\cos\phi = 0$$
$$0 \le \theta \le \frac{\pi}{3} \tag{3.10}$$

Similarly, in terms of ξ, ρ, θ variables,

$$f(\xi, \rho, \theta) = \sqrt{2}\xi \sin\phi + \sqrt{3}\rho \sin(\theta + \frac{\pi}{3}) + \rho \cos(\theta + \frac{\pi}{3}) \sin\phi - \sqrt{6}c\cos\phi = 0$$
$$0 \le \theta \le \frac{\pi}{3} \tag{3.11}$$

In terms of p and q, Mohr-Coulomb model is simply given as

$$F = R_{mc}q - p\tan\phi - c = 0 \tag{3.12}$$

where

$$R_{mc}(\Theta,\phi) = \frac{1}{\sqrt{3}\cos\phi}\sin(\Theta+\frac{\pi}{3}) + \frac{1}{3}\cos(\Theta+\frac{\pi}{3})\tan\phi \tag{3.13}$$

As shown in Figure 3.2a and Figure 3.2b, the yield function is a straight line in its meridian and the yield function has a shape of the irregular hexagon in the π-plane. Chen and Han (1989) states that some of the non-metallic materials like soil have a good compressive strength, under compressive forces with confining pressure, it may exhibit ductile and shear failure behavior. While under a tensile load, a brittle failure behavior with low tensile strength is expected. Thus, the Mohr-Coulomb criterion should be combined with the Rankine maximum tensile strength cutoff, to better analyze a hybrid shear-tensile failure behavior.

According to the documentation of Abaqus (2014), a commonly used plastic flow potential for the Mohr-Coulomb model is given as:

$$G = \sqrt{(\epsilon \qquad \overline{)^2 + (\mathrm{R}_{mw}\mathrm{q})^2}} - p\tan\psi \tag{3.14}$$

where

$$R_{mw}(\Theta,e) = \frac{1}{2}\frac{4(1-e^2)\cos^2\Theta + (2e-1)^2}{2(1-e^2)\cos\Theta + (2e-1)\sqrt{4(1-e^2)\cos^2\Theta + 5e^2 - 4e^2}}R_{mc}(\frac{\pi}{3},\phi) \tag{3.15}$$

and

$$R_{mc}(\frac{\pi}{3},\phi) = \frac{3-\sin\phi}{6\cos\phi} \tag{3.16}$$

ϵ is a parameter for meridional eccentricity, that defines the rate at which the hyperbolic function approaches the asymptote and e is a parameter for deviatoric eccentricity that describes the" out-of-roundness" of the deviatoric section in terms of the ratio between the shear stress along the extension meridian ($\Theta = 0$) and the shear stress along the compression meridian ($\Theta = \frac{\pi}{3}$).

The plastic flow potential for the Mohr-Coulomb yield surface in the meridional plane is shown in Figure 3.3.

(a) Meridian Plane (b) π - plane

Figure 3. 2 Graphical representation of the Mohr-Coulomb criterion in principal stress space, after Chen and Han (1989).

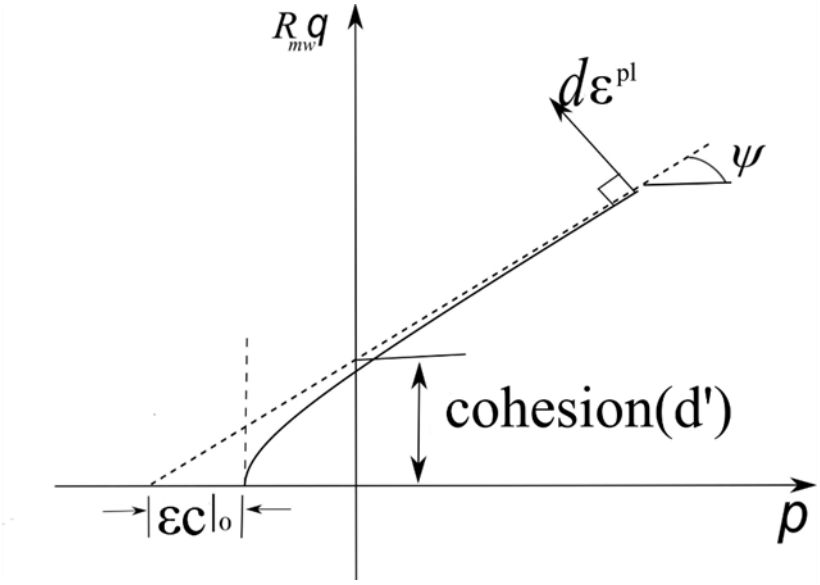

Figure 3. 3 Flow potentials in the meridional stress plane, after Abaqus (2014), Where ψ is the dilation angle.

3.2.3 Hyperbolic Drucker-Prager yield criterion

The hyperbolic Drucker-Prager yield criterion is the combination of the linear Drucker-Prager criterion and the maximum tensile stress condition of Rankine criterion, which is a generalized modification of the Von Mises criterion, by considering the influence of the hydrostatic stress component on failure given in Figure 3.4.

In the Mohr-Coulomb model, corners of the hexagon can cause a serious problem. In this regard, the Drucker-Prager model is a smooth approximation to the Mohr-coulomb criterion, which can be matched by adjusting the cone size. The original linear model was mainly used where most of the stresses are compressive in nature. However, if the tensile stress is involved, a

tensile cut-off should be included. That's why the hyperbolic Drucker-Prager yield criterion come out.

The hyperbolic Drucker-Prager yield criterion is given by the following function Abaqus (2014):

$$F = \sqrt{\left(d' - \sigma_t \tan\beta\right)^2 + q^2} - p' \tan\beta - d' = 0 \tag{3.17}$$

where F is the isotropic yield function; σ_t is the tensile strength; β and d are the friction angle and cohesion in $p' - q$ space, respectively; and d' is related to d by:

$$d' = \sqrt{\left(d' - \sigma_t \tan\beta\right)^2 + d^2} \tag{3.18}$$

In this study, a non-associated flow rule is used, and the plastic potential function shown in Figure 3.5 is expressed as:

$$G = \sqrt{\left(\omega d' \tan\psi\right)^2 + q^2} - p' \tan\psi \tag{3.19}$$

where ω is a parameter, referred to as the eccentricity, that defines the rate at which the function approaches the asymptote (the flow potential tends to a straight line as the eccentricity tends to be zero, we give a value of 3 to ω herein).

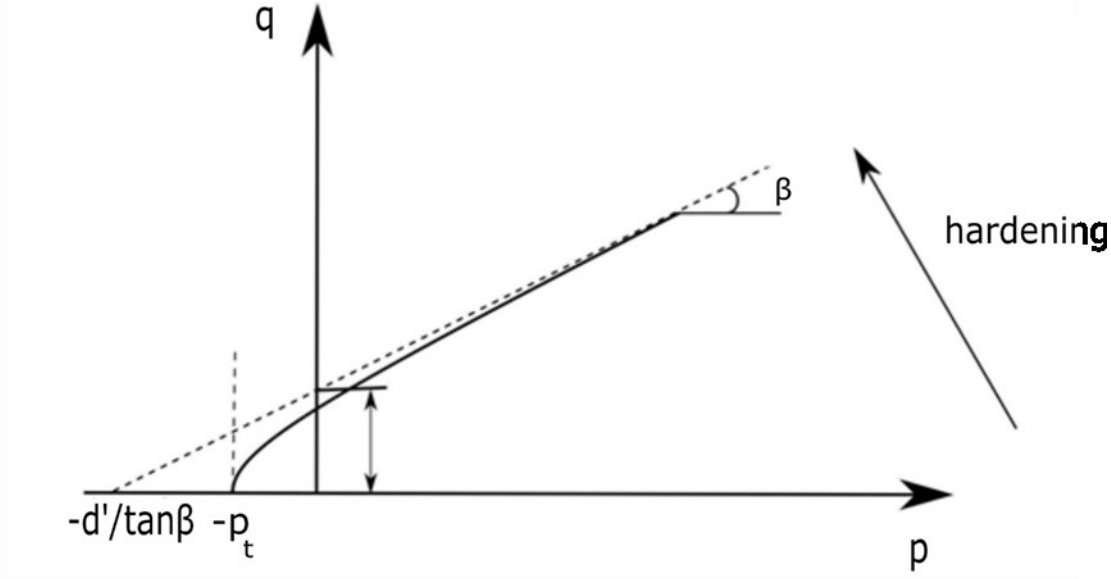

Figure 3. 4 Yield surface of the hyperbolic Drucker-Prager model in the meridian plane, after Abaqus (2014).

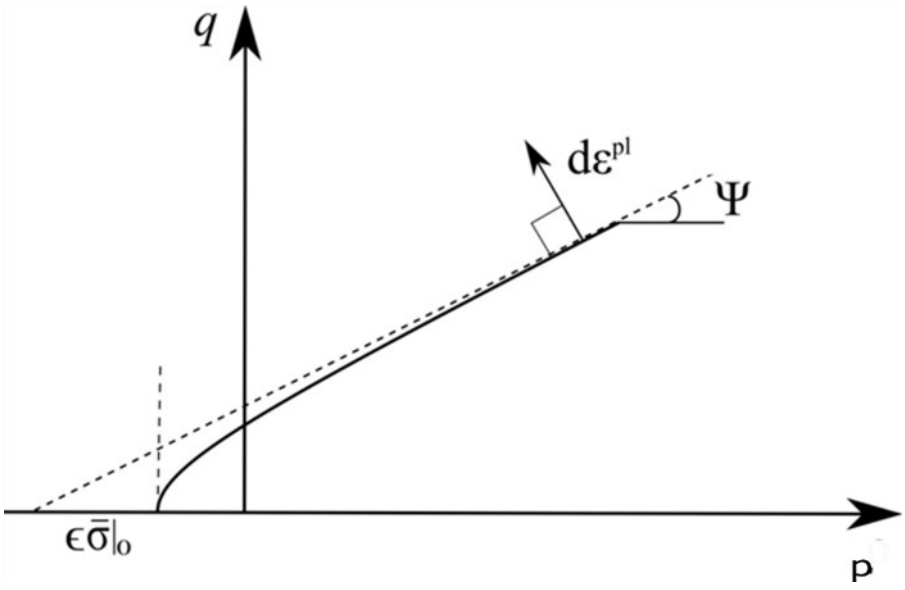

Figure 3. 5 Plastic flow potential in the meridian plane, after Abaqus (2014).

3.3 A comparison among different models

Geotechnical engineering projects like pipeline engineering, tunnels, and embankments can be treated in a plane strain stress condition. Therefore, the constitutive model parameters are often matched to provide the same flow and failure response in the plane strain condition.

The linear Drucker-Prager flow potential defines the plastic strain increment as:

$$d\varepsilon^{pl} = d\bar{\varepsilon}^{pl} \frac{1}{(1-\frac{1}{3}\tan\psi)} \frac{\partial}{\partial\sigma}(q - p\tan\psi) \tag{3.20}$$

where $\bar{\varepsilon}^{pl}$ is the equivalent plastic strain increment.

Assume plane strain in the 1-direction with $d\varepsilon_1^{pl} = 0$, which provides the constraint

$$\sigma_1 = \frac{1}{2}(\sigma_2 + \sigma_3) - \frac{1}{3}\tan\psi q \tag{3.21}$$

Using this constraint, we can rewrite p and q in terms of the principal stresses in the plane of deformation as:

$$q = \frac{3\sqrt{3}}{2\sqrt{9 - \tan^2 \psi}}(\sigma_2 - \sigma_3) \tag{3.22}$$

and,

$$p = -\frac{1}{2}(\sigma_2 + \sigma_3) + \frac{\tan\psi}{2\sqrt{3(9 - \tan^2 \psi)}}(\sigma_2 - \sigma_3) \tag{3.23}$$

Accordingly, the Drucker-Prager yield surface can be written in terms of σ_2 and σ_3 as

$$\frac{9 - \tan\beta\tan\psi}{2\sqrt{3(9 - \tan^2 \psi)}}(\sigma_2 - \sigma_3) + \frac{1}{2}\tan\beta(\sigma_2 + \sigma_3) - d = 0 \tag{3.24}$$

and, the Mohr-Coulomb yield surface in (2,3) plane is

$$\sigma_2 - \sigma_3 + \sin\phi(\sigma_2 + \sigma_2) - c\cos\phi = 0 \tag{3.25}$$

by comparing Eq. 3.24 and Eq. 3.25, we can derive into:

$$\sin\phi = \frac{\tan\beta\sqrt{3(9 - \tan^2 \psi)}}{9 - \tan\beta\tan\psi} \tag{3.26}$$

$$c\cos\phi = \frac{\sqrt{3(9-\tan^2\psi)}}{9-\tan\beta\tan\psi}d \tag{3.27}$$

These relationships provide a match between Mohr-Coulomb material parameters and Drucker-Prager material parameters in-plane strain. There are two extreme cases of flow definition:

(a) Associated flow, $\psi = \beta$

(b) Non-dilatant flow, $\psi = 0$

For our case, we will use the Eq. 3.26, to determine Drucker-Prager friction angle β and Eq. 3.27, to determine Drucker-Prager cohesion strength parameter *d*, by considering dilation and non-associated flow behavior. A comparison of different yield criterion functions in the π plane is given in Figure 3.6.

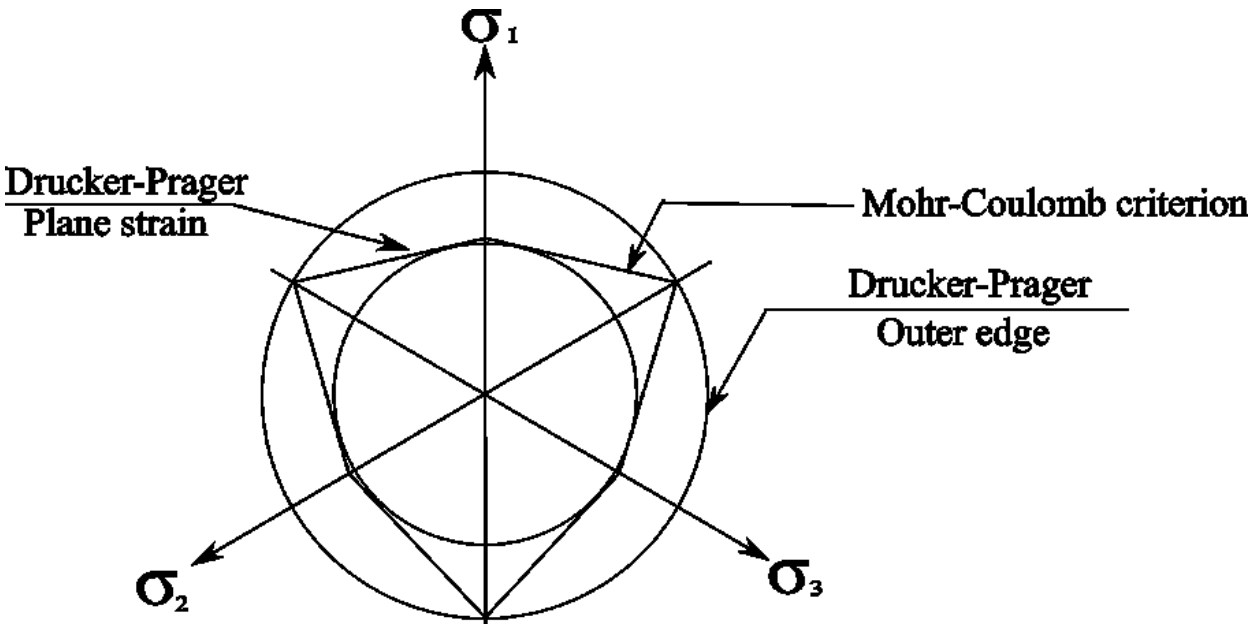

Figure 3. 6 The π plane section of the Mohr-Coulomb surface and the Drucker-Prager approximations, modified after Neto et al. (2008).

3.4 Temperature-dependent mechanical properties

The behavior of soil at room temperature or below room temperature in the frozen stage has been studying by various researchers. But very few research has been conducted to study the complex behavior of soils' mechanical strength parameters, when the soil temperature varies below and above 0^{o} C. All the mechanical strength curves of soil behave non-linearly with respect to temperature when the temperature is near to 0^{o} C and this non-linearity remains until the temperature drops below - 4^{o} C, behind which the mechanical strength parameters curve gives a linear pattern with respect to temperature. Such a nonlinear correlation should be closely related to the temperature dependent unfrozen water content in the frozen soil.

A research work by Nixon (1991) gives a relationship between unfrozen water content and temperature by a non-linear power law equation $W_u = A\ (-T)^B$. The reason behind this nonlinear effect may be because of sticky and adhesive nature of frozen water content, which increases the cohesive properties of soil. This phenomenon can be illustrated in Figure 3.7a for various clays and Figure 3.7b for various silts. A transition zone exists between the available unfrozen water content and the maximum frozen water content. The available free water in soil keep on freezing with the temperature drop until the temperature of - 4° C, but as the temperature drops below this critical temperature, there is no more drop in the unfrozen water content amount in both clays and silts. The amount of unfrozen water after temperature dropping below - 4° C in clay is more than the silts, the reason might be the inter-layer water in clay minerals which still behave viscously at very low temperature. The non-linear behavior in frozen water content leads to the nonlinearity in the mechanical strength parameters (e.g., tensile strength, uniaxial compression, modulus of elasticity, and cohesion) with respect to temperature give in the literature (Azmatch et al. 2010, 2011; Chen et al. 2011; Esmaeili-Falak et al. 2018; Hu et al. 2013; Li and Zhu 2003; Nixon 1991; Seo and Choi 2012; Zhou et al. 2015).

The tensile strength of soil increases with the drop in temperature as shown in Figure 3.8a & b, Figure 3.9a & b. The combined plot for the tensile strength of various types of soils available in the literature is drawn in Figure 3.10. The demonstration of theses plots concludes that when the temperature is between - 4° C and 0° C, there is non-linearity in the relationship between the tensile strength and temperature. But when the temperature drops below - 4° C, the relationship curves becomes linear. And, in Figure 3.9a and Figure 3.9b, plotted for the literature data available in (Azmatch et al. 2011; Seo and Choi 2012) shows that tensile strength not only

depends on the temperature but also strain rate. Higher strain rate will yield to higher tensile strength and lower strain rate gives low tensile strength.

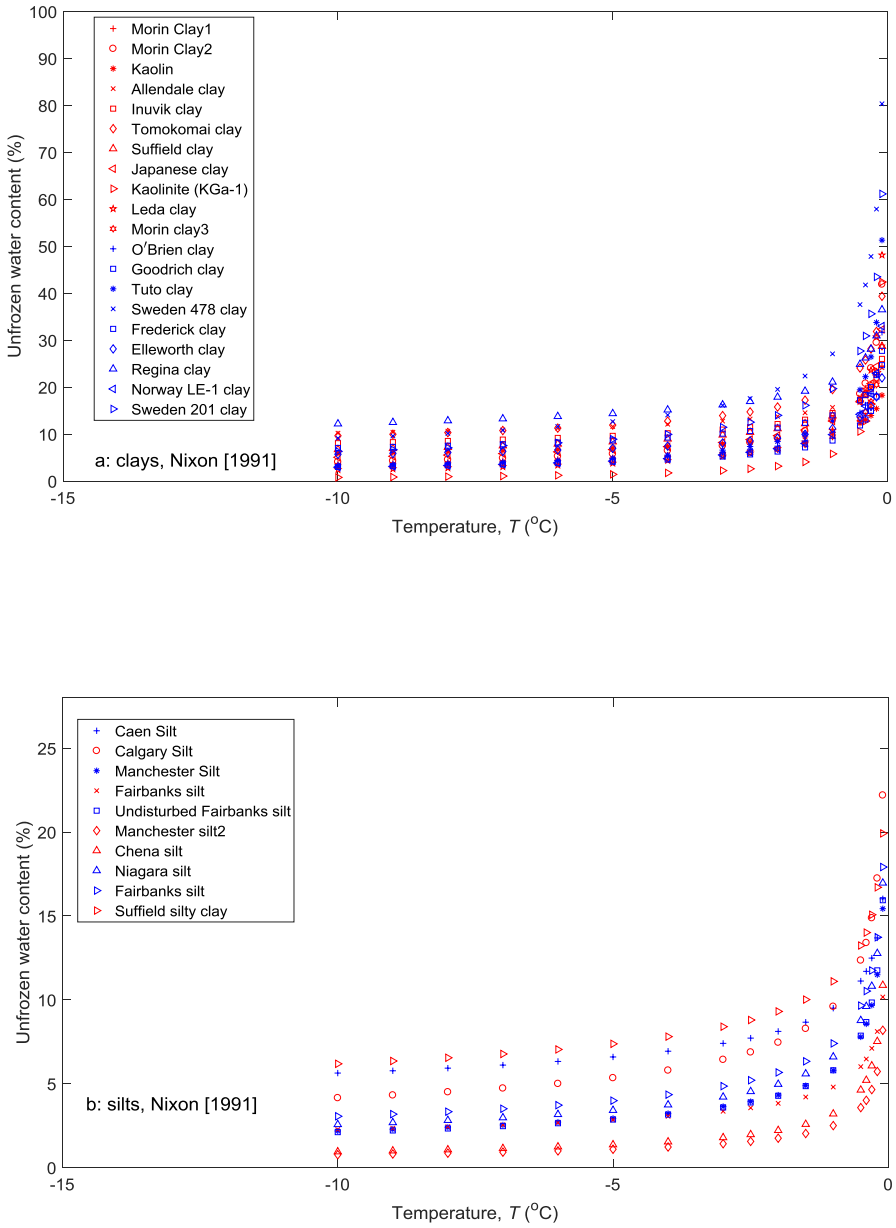

Figure 3. 7 Graphs showing unfrozen water content of (a) clays and (b) silts at varying frozen temperatures, after Nixon (1991).

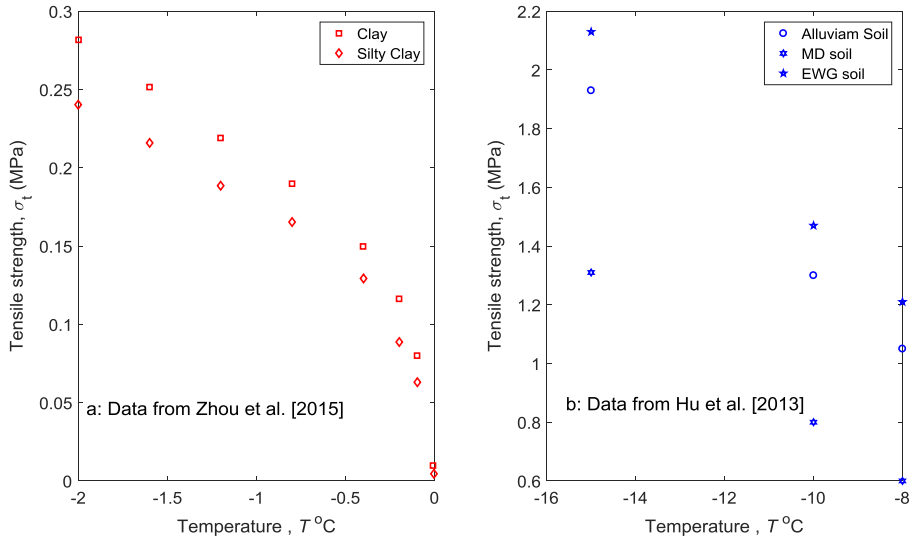

Figure 3. 8 Plots of (a) tensile strengths of clay and silty clay with respect to frozen temperature, and (b) tensile strengths of marine deposit, weak granite and alluvium soil with respect to frozen temperature.

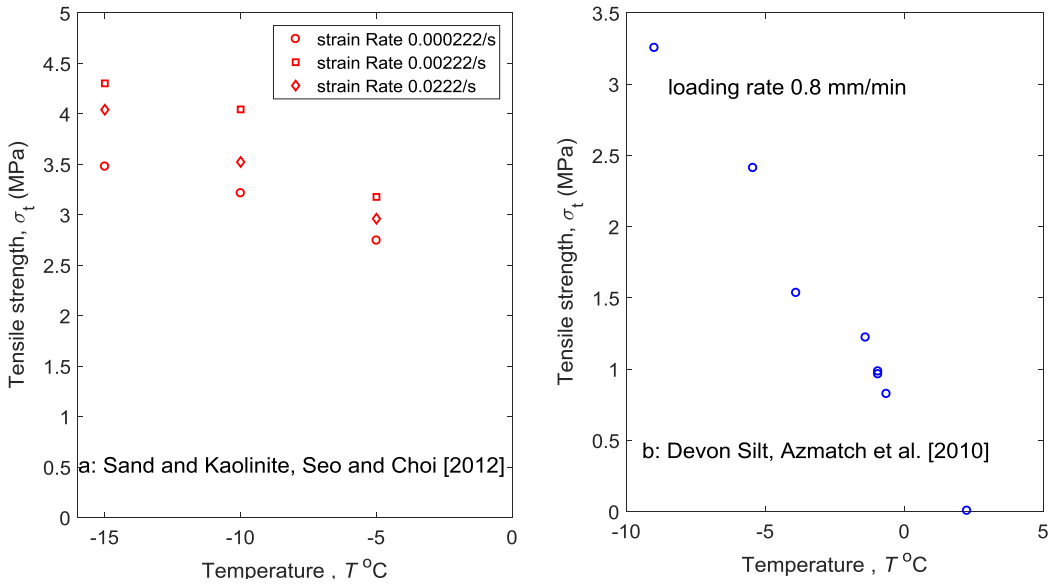

Figure 3. 9 (a) Tensile strength of sand and kaolinite with respect to frozen temperature, after Seo and Choi (2012) and (b) tensile strength of Devon silt with respect to frozen temperature, after Azmatch et al. (2010).

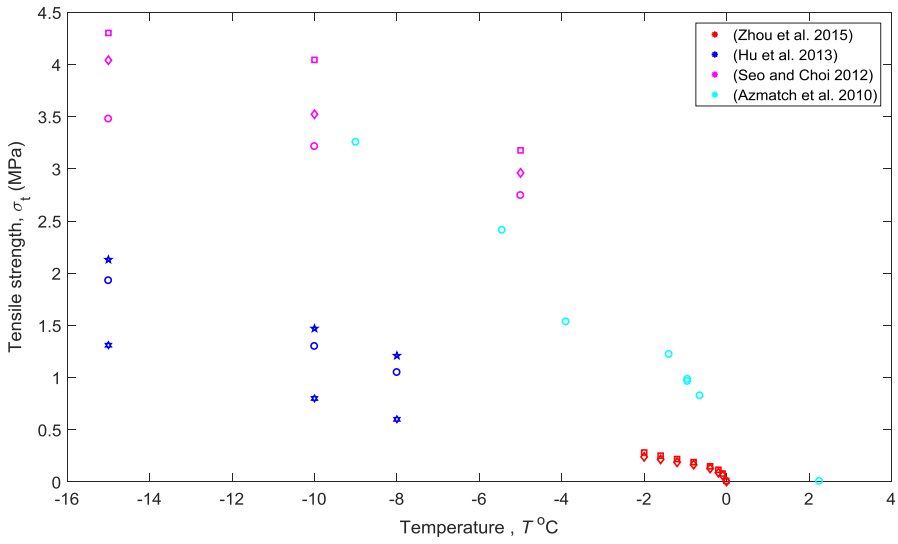

Figure 3. 10 Tensile strength of the various type of soils with respect to frozen temperature.

Uniaxial compressive strength parameter behavior with respect to temperature can be illustrated in Figure 3.11a & b and Figure 3.12a & b. The relation of the uniaxial compression strength parameter with respect to temperature is also affected by the availability of unfrozen water content. When the temperature is above - 4 ^{o}C, a non-linear behavior is produced in the strength parameter curve with respect to temperature. But as the temperature drops below - 4 ^{o}C, the relationship between temperature and compressive strength parameter becomes linear and gives straight plot. From Figure 3.11a and Figure 3.12a & b, it is determined that compressive strength parameter is also strained dependent. The compressive strength plot will give higher values with respect to frozen temperature at higher strain rate while at a lower strain rate, it yields lower values for compressive strength.

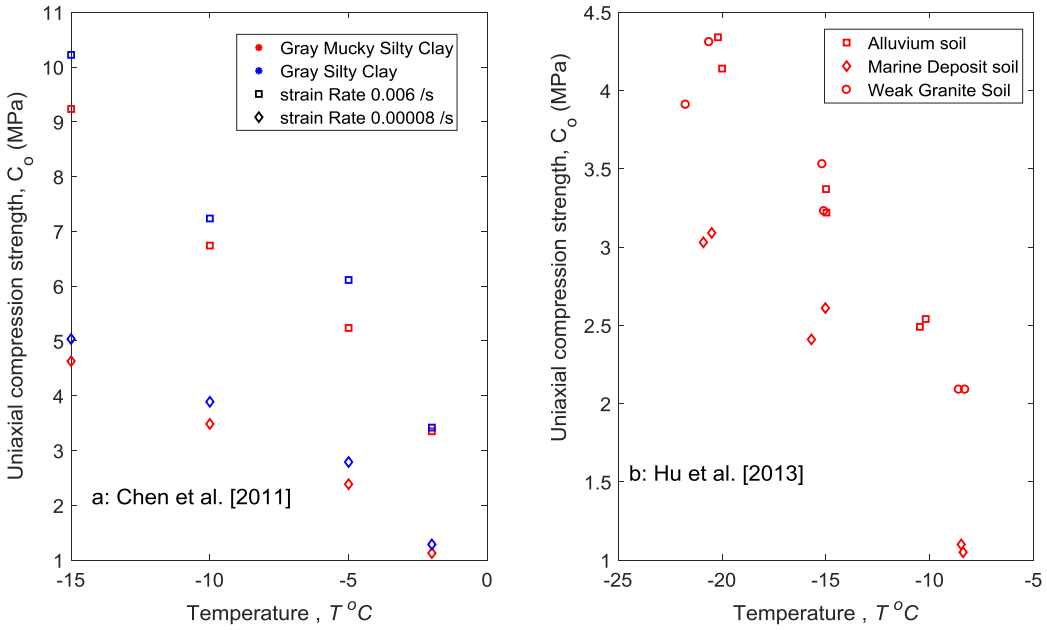

Figure 3. 11 (a) Uniaxial compression strength of Silty clay with respect to temperature, after Chen et al. (2011) and (b) Uniaxial strength of Alluvium, Marine Deposit and Weak granite soil with respect to temperature, after Hu et al. (2013).

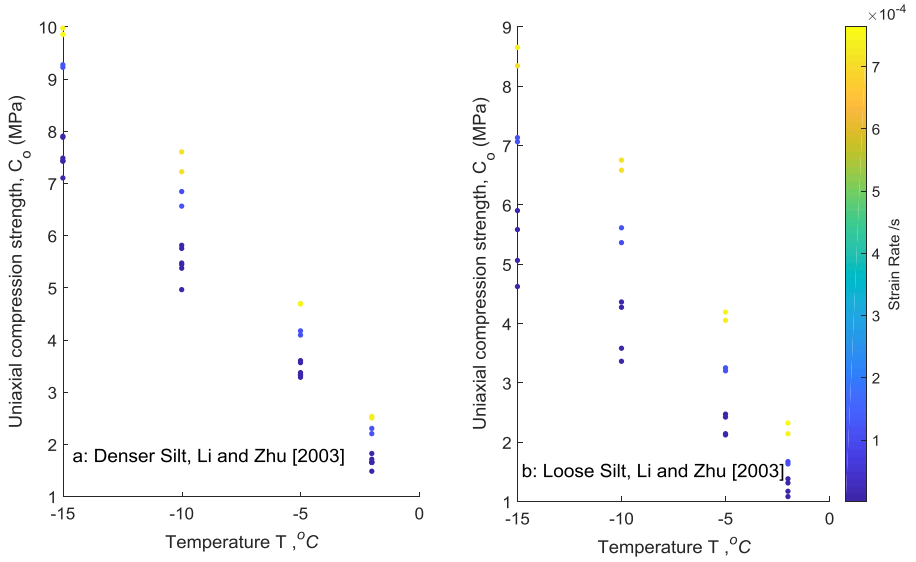

Figure 3. 12 Strain rate dependent uniaxial compression strength of silts with respect to temperature, after Li and Zhu (2003).

Young's modulus of elasticity also increases with the decrease of temperature. A modulus of elasticity gives linear relationship plots with respect to temperature exists as the temperature drops below – 4 ºC. But the relationship curve remains non-linear with respect to the temperature as the temperature is above – 4 ºC shown in Figure 3.13 to Figure 3.16. Young's modulus of elasticity is also strain dependent shown in Figure 3.13a, Figure 3.14b and Figure 3.15a & b, higher strain rate results in higher elastic strength values while lower strain rate yields in lower elastic strength values.

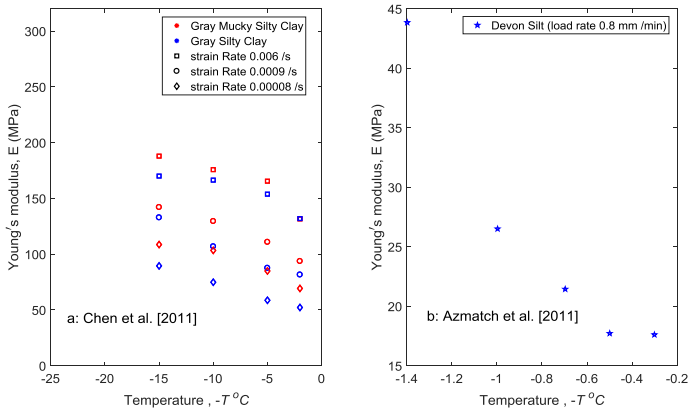

Figure 3. 13 (a) Young's modulus of gray silty clay with respect to frozen temperature, after Chen et al. (2011) and (b) Young's modulus of elasticity of Devon silt with respect to frozen temperature, after Azmatch et al. (2011).

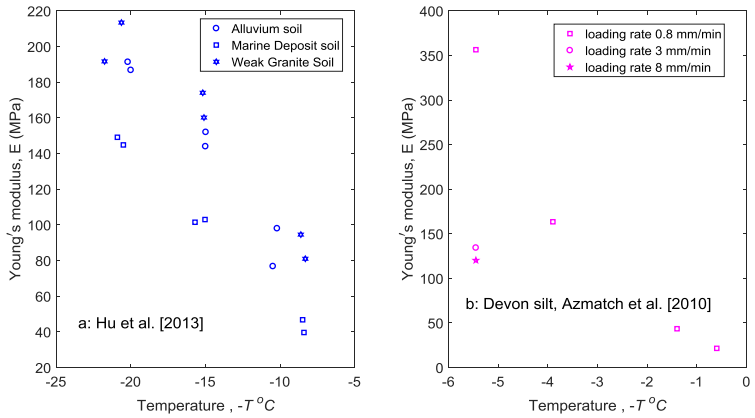

Figure 3. 14 (a) Young's modulus of Alluvium, Marine Deposit and Weak Granite soil with respect to frozen temperature, after Hu et al. (2013) and (a) Young's modulus of Devon silt with respect to frozen temperature, after Azmatch et al. (2010).

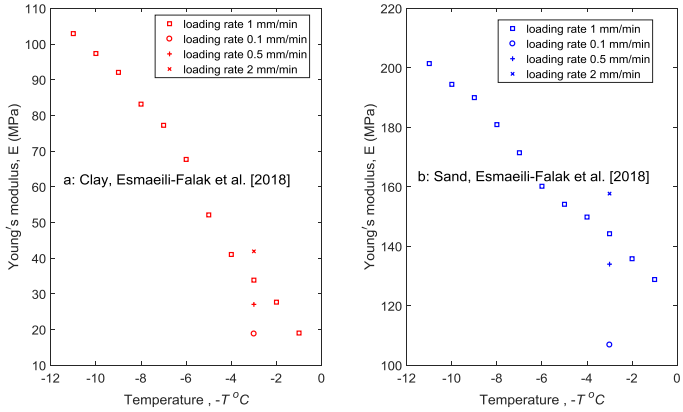

Figure 3. 15 (a) Young's modulus of lean clay with respect to frozen temperature and (b) Young's modulus of poorly graded sand with respect to frozen temperature, after Esmaeili-Falak et al. (2018).

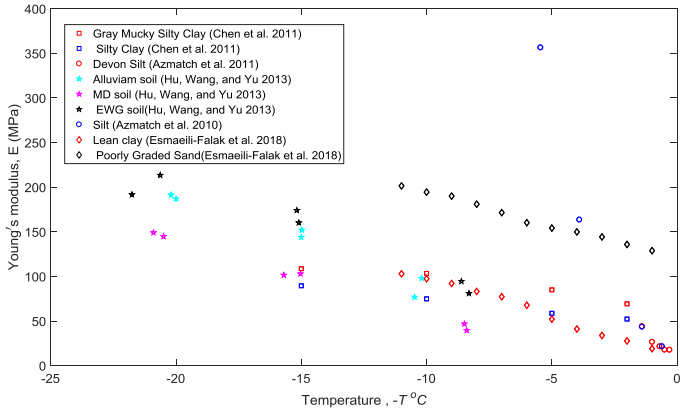

Figure 3. 16 Young's modulus of various types of soil with respect to frozen temperature.

The poisson rate of frozen soil is also temperature dependent as shown in (Figure 3.17). Poisson ratio increases with the decrease in a temperature, but this increase is not as dominant as other mechanical strength parameters.

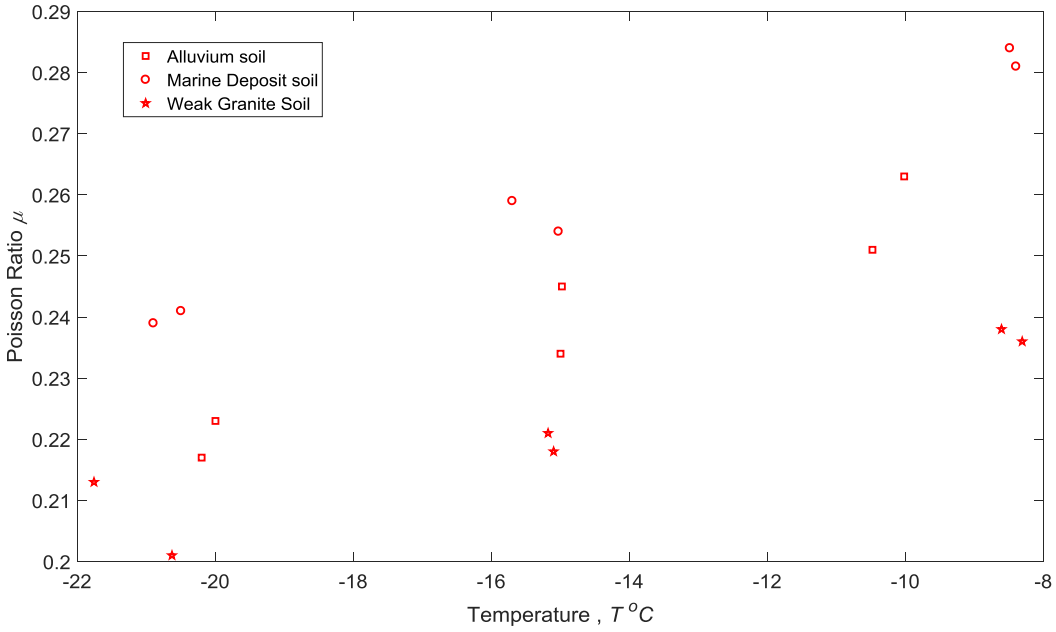

Figure 3. 17 Poisson's ratio of Alluvium, Marine Deposit and Weak Granite soil with respect to frozen temperature, after Hu et al. (2013).

3.3 Summary

- To have a better analysis in the geo-mechanical analysis, the Mohr-Coulomb yield criterion should be used with the Rankine maximum tensile strength yield criterion to consider the tensile yielding behavior.
- As a generalized modification of Von Mises criterion, the Drucker-Prager produces a smooth curve in principal stresses plane and minimize the efforts may use for theoretical numerical calculations of Mohr-Coulomb's hexagon surface. A hyperbolic Drucker-Prager model can be a considerable choice to consider the tensile yielding behavior. For a

plane strain condition, the Drucker-Prager model or the hyperbolic Drucker-Prager model inscribes the hexagon of Mohr-Coulomb yield surface in π-plane. Thus, the hyperbolic Drucker-Prager gives more conservative results during geo-mechanical analysis if it is applied in the plane strain condition with matched parameters from the Mohr-Coulomb model.

- The availability of maximum frozen water content affects the mechanical strength parameters of frozen soil relation with respect to frozen temperature. At the temperature – 4 ^{o}C, available water content keeps on freezing to a possible maximum freezing of water quantity and the temperature drops below this point, has no more effect on the unfrozen water content. This stage of temperature gives transition between linear and non-linear relation between temperature and mechanical strength parameters. Frozen water content improves the cohesive strength of soil while the friction angle almost remains unaffected. The mechanical strength parameters are also strain rate dependent, higher strain rate will give higher values for mechanical strength while lower strength parameters value will yield at lower strain rate. Poisson ratio decreases with a drop of temperature.

CHAPTER 4

NUMERICAL ANALYSIS OF PIPELINE UPLIFT RESISTANCE IN FROZEN CLAY

4.1 Governing equations

The frozen soil-pipe interaction simulation uses a coupled Thermal-Mechanical (TM) finite element formulation to consider the interactions between heat transfer and mechanical deformation and failure. The mechanical governing equations can be formulated as:

$$\sigma_{ij,j} + \rho b_i = 0 \tag{4.1}$$

$$\sigma_{ij} = C_{ijkl}\varepsilon_{kl} \tag{4.2}$$

$$\varepsilon_{ij} = \frac{1}{2}\left(\frac{\partial u_i}{\partial x_j} + \frac{\partial u_j}{\partial x_i}\right) \tag{4.3}$$

where σ_{ij} is the stress tensor, $\boldsymbol{b_i}$ is the body force, C_{ijkl} is the elastic stiffness tensor, ε_{kl} is the strain tensor, $\vec{\boldsymbol{u}}$ is the displacement vector.

And in the absence of internal heat generation, the heat conduction is described by the Fourier's equation:

$$\frac{\partial^2 T}{\partial x^2} + \frac{\partial^2 T}{\partial y^2} + \frac{\partial^2 T}{\partial z^2} = \frac{1}{k}\frac{\partial T}{\partial t} \tag{4.4}$$

where T is a temperature, t is a time, and k is a thermal diffusivity.

The constitutive models for the failure criterion have been given in Chapter 3. The equivalent plastic strains in tensile yielding on the tension cut-off yield surface and shear yielding is given in Eq. 4.5 and Eq. 4.6 respectively for the Mohr-Coulomb criterion (Abaqus, 2014) and the equivalent plastic strain (PEEQ) for the Hyperbolic Drucker-Prager criterion (Abaqus, 2014) is given in Eq. 4.7.

$$\bar{\varepsilon}_t^{pl} \tag{4.5}$$

$$\bar{\varepsilon}^{pl} = \int \frac{1}{c}\sigma : d\varepsilon^{pl} \tag{4.6}$$

$$\bar{\varepsilon}^{pl} = \int \frac{\sigma : d\varepsilon^{pl}}{d'} \tag{4.7}$$

4.2 Temperature-dependent mechanical properties of a frozen clay

There is a very limited database for the temperature-dependent mechanical properties of frozen clay soils which both cover the compressive strength properties and the tensile strength. The only one available is the Hong Kong Marine Deposits soil (HKMD), for which the temperature-dependent mechanical properties were provided by Hu et al. (2013). This kind of marine deposits soil was encountered during construction of the huge project of tunneling, passing through the marine environment where an approach of artificially frozen technique is applied. The measured temperature-dependent mechanical properties of Hong Kong Marine Deposits soil will be applied in this study to investigate frozen soil-pipe interaction at varying temperatures.

$$0.8\psi = \phi - \phi_{cri} \tag{4.8}$$

$$c = 2C_0 \frac{\cos\phi}{1-\sin\phi} \tag{4.9}$$

The basic physical properties, mineralogy, strength, and thermal properties of HKMD are included in Table 4.1. Among them, the shear strength, and dilation angle parameters, and residual friction angle of the Hong Kong marine deposits soils are determined based on clay content by using the nonlinear relationship model provided in Li and Wong (2016) and given in Table 4.1. The dilation angle is determined by Eq. 4.1 given by Bolton (1986) and Drucker-Prager model friction angle β is determined by the Eq. 3.26 given in Table 4.1. Thermal material properties of the Hong Kong Marine Deposits soil are also given in Table 4.1. The measured mechanical properties of HKMD at different temperatures are provided by Hu et al. (2013). The data was used to determine the required strength parameter values using nonlinear regression power law interpolation as shown in Table 4.2. The derived mechanical strength parameters-temperature relations are shown in Figure 4.1a, b, c, and d. A Ducker-Prager cohesion strength parameter is determined by Eq. 3.27 and cohesion strength parameter for Mohr-Coulomb is determined by Eq. 4.2 given by Fjær et al. (2008). The non-linear response of soil strength parameters when the temperatures drop around – 4 ºC, shown in these graphs, has already been discussed in detail in the previous chapter. Since the mechanical properties of frozen clay soils also depend on the applied strain rate, the lower bound of strength parameters (the one from the lowest strain rate) are selected in the numerical analysis herein.

Table 4. 1 Multi-physical properties of Hong Kong marine deposit soil.

Physical property	**Unit**	**Values**	**Reference**
Water content	%	57	Yin (1999, 2001)
Dry density	kg/m^3	1200	Yin (1999, 2001)
Bulk Density	kg/m^3	1700	Yin (1999)
Specific gravity	-	2.66	Yin (1999, 2001)
Clay content	%	28	Yin (1999)
Silt content	%	46	Yin (1999)
Fine Sand content	%	26	Yin (1999)
PL	%	29	Yin (1999)
LL	%	60	Yin (1999)
PI	%	31	Yin (1999)
Peak friction angle, ϕ_{max}	degrees	28	Li and Wong (2016)
Residual friction angle, ϕ_{cri}	degrees	21.9	Li and Wong (2016)
Dilation angle, ψ	degrees	7.6	Bolton (1986)
DP friction angle β	degrees	38	(Equation 3.26)
Specific heat capacity	KJ/ (kg ^oC)	1.28	Leung et al. (2012)
Thermal conductivity at -15 ^oC	W / (m K)	1.865	Leung et al. (2012)

Table 4. 2 Nonlinear equations for temperature-dependent mechanical properties of frozen Hong Kong marine deposit soil.

No.	Strength Parameter	Equation	A	B	R^2
1	Young's modulus	$E = A(-T)^B$	2.6758	1.3243	0.994
2	Poisson's ratio	$\mu = A(-T)^B$	0.1129	-0.1771	0.977
3	Uniaxial compression strength	$C_0 = A(-T)^B$	0.1251	1.0655	0.952
4	Tensile strength	$\sigma_t = A(-T)^B$	1.233	1.233	0.999

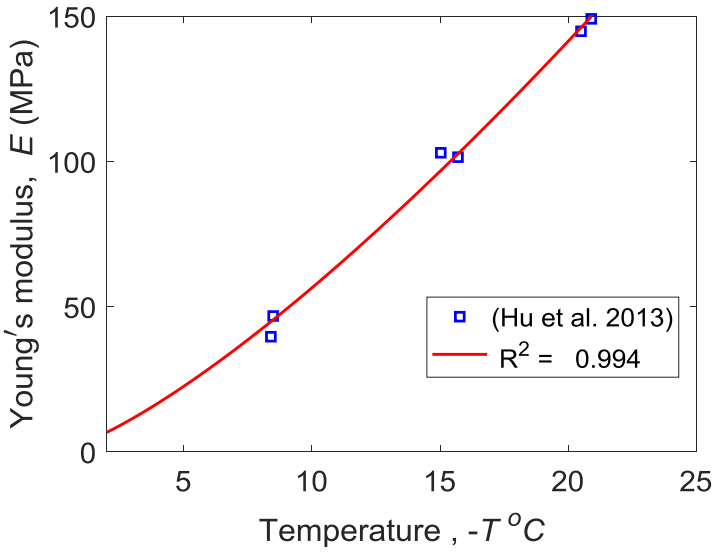

(a) Young's modulus vs temperature

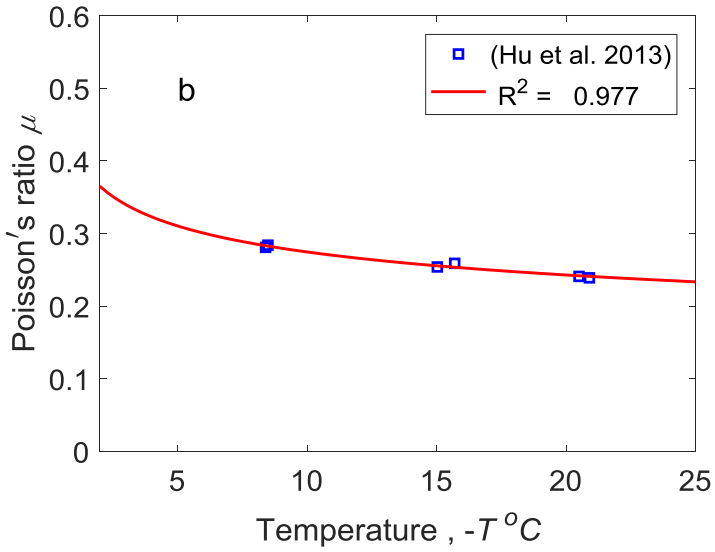

(b) Poisson's ratio vs temperature

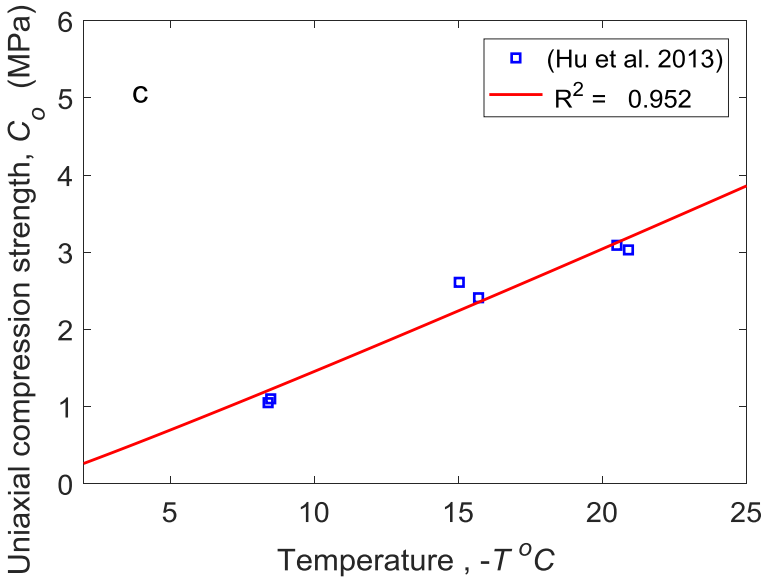

(c) Uniaxial compression strength vs temperature

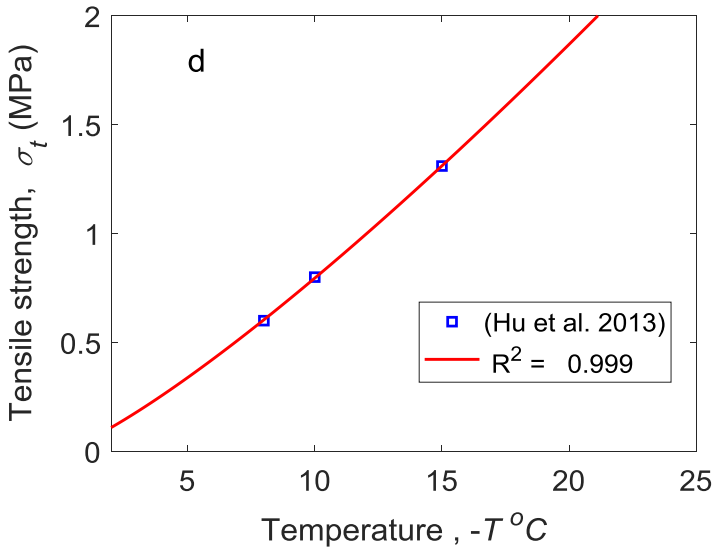

(d) Tensile strength vs temperature

Figure 4. 1 Relationship between the strength parameters (a) Young's modulus, (b) Poisson's ratio, (c) Uniaxial compressive strength, and (d) Tensile strength of frozen soil with respect to frozen temperature (-*T*) ^{o}C

4.3 FEM analysis of soil-pipe interactions at constant frozen temperatures

4.3.1 Configuration and FEM mesh

Treated as a plane strain problem, the dimensions of the frozen soil block through which the pipe passes are shown in Figure 4.2a. The selection of soil block dimensions and position of pipe is based on the laboratory testing performed by (J.F. Nixon, 1998; Wong et al., 2016) and the outcomes of their study showing promising and effective results. The soil block was divided into possible small meshes to avoid any convergence issues and without the distortion of any

elements in the body, as shown in Figure 4.2b. For analyses purpose, four monitoring points were selected in a different location of soil around the pipe as shown in Figure 4.2c. Soil block was divided into 1120 mesh elements having CPE3T triangular shape and pipe was divided into 164 elements having CPE3 triangular shape. The diameter of the pipe is kept 150 mm and thickness 20 mm. The convergence of output results was checked to analyses the deviation in terms of bearing capacity and strains in a system. It was determined that on further making the mesh finer yields no more significant effects.

Both the Mohr-Coulomb model with the Rankine tensile cut and the hyperbolic Drucker-Prager model were used in the constitutive analysis. The inputs of parameters are based on the data in Tables 4.1 and 4.2. The conversion of parameters at a plane-strain condition has been discussed in detail in Chapter 3. Thermal expansion is ignored in current study formulations as the temperature varies from - 15 ^{o}C to - 2 ^{o}C during heat transfer stage in frozen soil leaving not considerable expansion effect on the thermal elastic strain of the frozen soil because most of the available water content has already been frozen at temperature - 2 ^{o}C. Those models are available in finite element analysis software, Abaqus. Our task is to investigate the failure process in the frozen soil around pipes at varying temperature conditions. We also need to figure out which criterion gives more realistic and promising result in analyzing the uplift resistance of pipe buried in frozen soils.

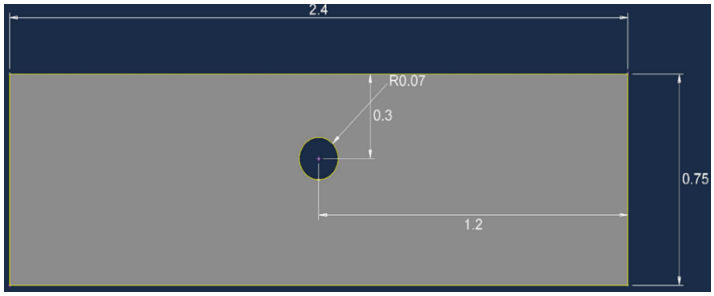

(a)

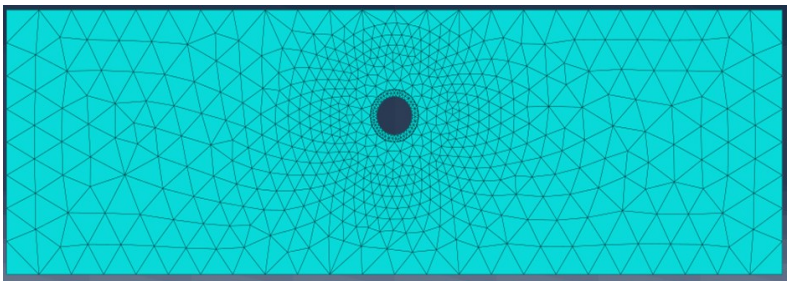

(b)

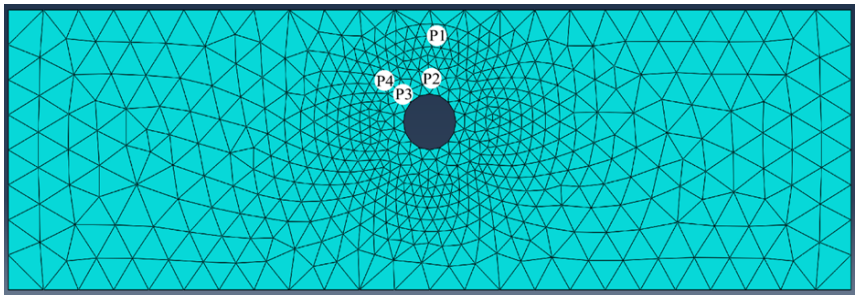

(c)

Figure 4. 2 (a) Dimension (unit is m), (b) mesh, and (c) four monitoring points for the FEM.

4.3.2 Uplift resistance and plastic strain

For the displacement-controlled failure analysis of frozen soil, vertical displacements (U2) of 4.2 cm, 4.5 cm, and 4.9 cm were invoked at - 2 ºC, - 5 ºC and - 10 ºC respectively using Mohr-Coulomb with Rankine cut-off failure criterion and Hyperbolic Drucker-Prager failure criterion approaches for the numerical analyses of pipeline as shown in Figures 4.3 to 4.5.

The contours are given in Figure 4.3a and b, Figure 4.4a and b and Figure 4.5a and b indicate that Hyperbolic Drucker-Prager model produces larger values of vertical displacement at critical points as compared to the result from Mohr-Coulomb model with Rankine cut-off.

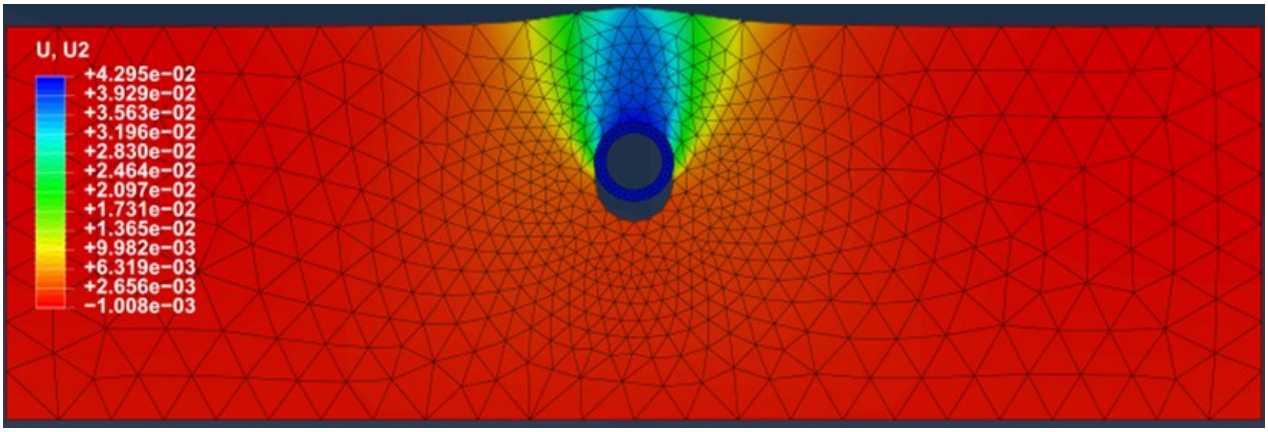

(a) Mohr-Coulomb model with tensile cut off, T = -2 ^{o}C

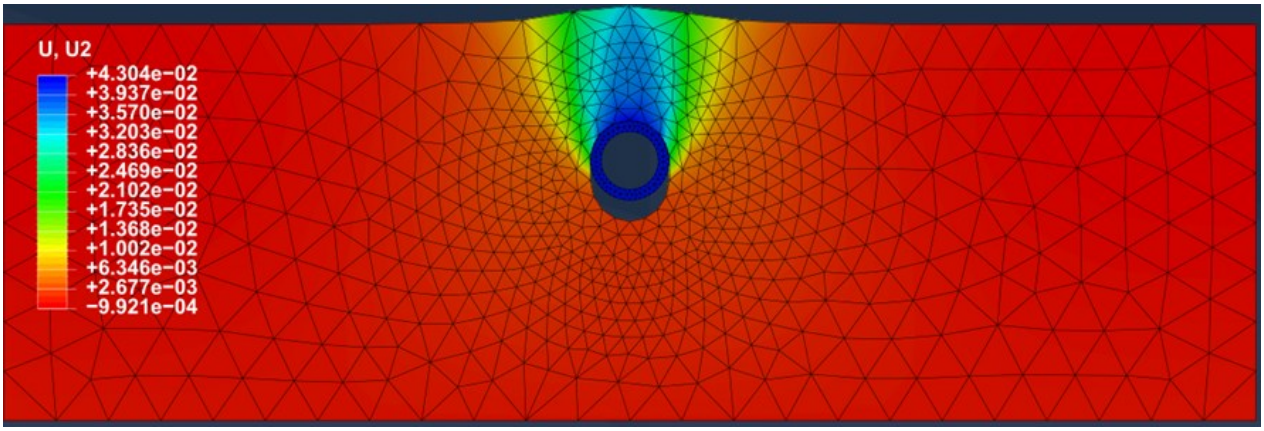

(b) Hyperbolic Drucker- Prager model, T = -2 ^{o}C

Figure 4. 3 Figure 4.6: Contour of uplift vertical displacement (U2) in Pipeline by using (a) Mohr-Coulomb model with tensile cut-off, and (b) Hyperbolic Drucker- Prager model at T = - 2 ^{o}C.

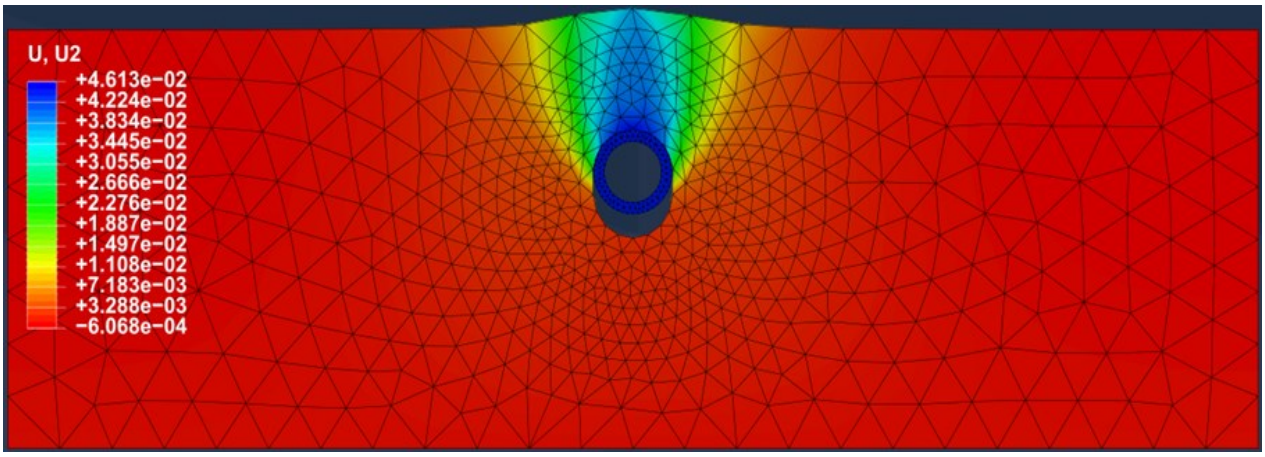

(a) Mohr-Coulomb model with tensile cut off, T = - 5 ^{o}C

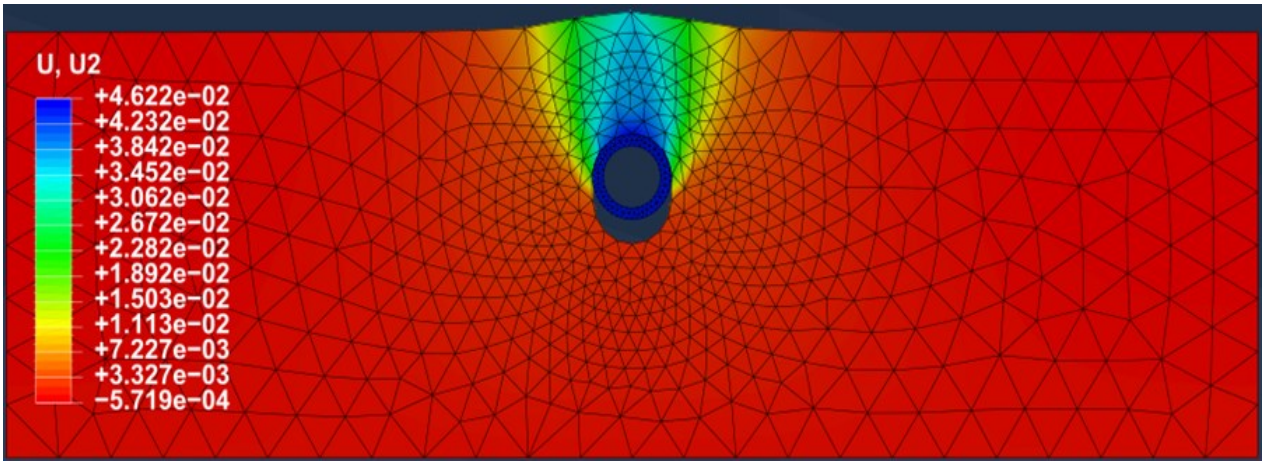

(b) Hyperbolic Drucker- Prager model, T = - 5 ^{o}C

Figure 4. 4 Contour of uplift vertical displacement (U2) in Pipeline by using (a) Mohr-Coulomb model with tensile cutoff, and (b) Hyperbolic Drucker- Prager model at T = - 5 ^{o}C.

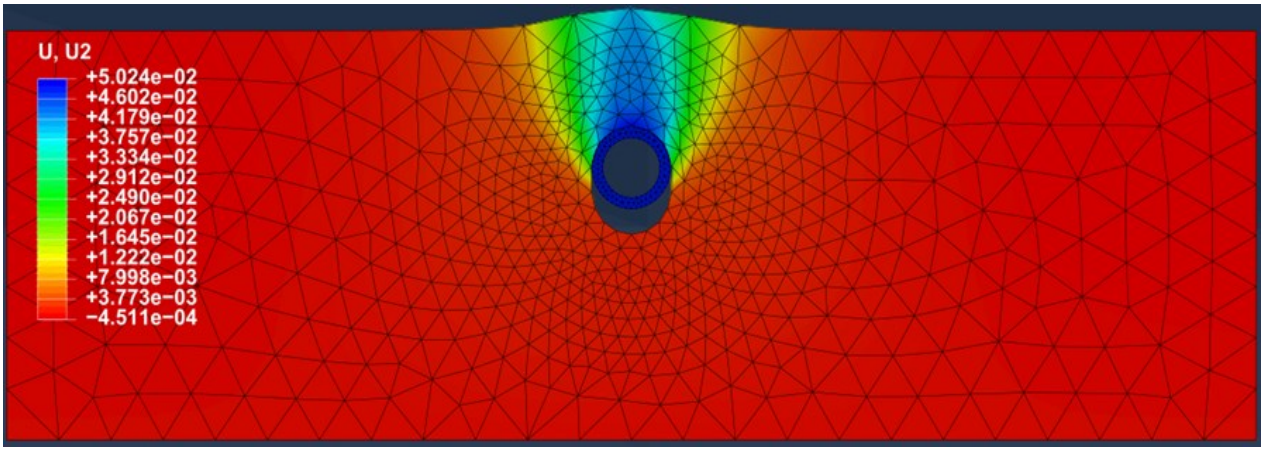

(a) Mohr-Coulomb model with tensile cut off, T = - 10 ºC

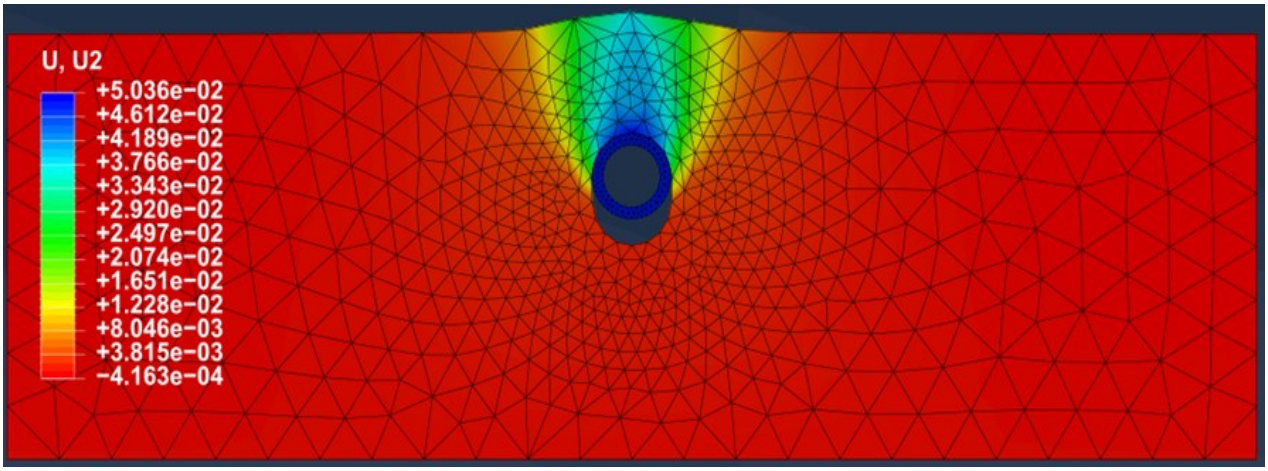

(b) Hyperbolic Drucker- Prager model, T = - 10 ºC

Figure 4. 5 Contour of uplift vertical displacement (U2) in Pipeline by using (a) Mohr-Coulomb model with tensile cutoff, and (b) Hyperbolic Drucker- Prager model at T = - 10 ºC.

The frozen clay shows more reaction or resistance towards the uplift displacement with respect to a lower temperature. The lower the temperature the higher the resistance force and a larger displacement of pipe will be required to cause failures in the frozen clay soil as shown in Figure 4.6.

At - 2 ^{o}C, the frozen clay reaches to failure stage at a displacement of 4.2 cm with a maximum resistance force of 38.35 kN and 37.23 kN, respectively, for the model of Mohr-Coulomb model with Rankine tensile cut-off and the Hyperbolic Drucker-Prager model. At - 5 ^{o}C, the frozen clay reaches to failure stage at a displacement of 4.2 cm with a maximum resistance force of 110.1 kN and 104.6 kN for those two models. At – 10 ^{o}C, a maximum resistance force of 238.9 kN and 228.1 kN can be achieved. The numerical analysis of both failure criterion for reaction forces shows that before reaching to failure stage, the hyperbolic Drucker-Prager model displays a slight drop in the bearing capacity, while the Mohr-Coulomb model shows a continuous increase in reaction force until soil fails.

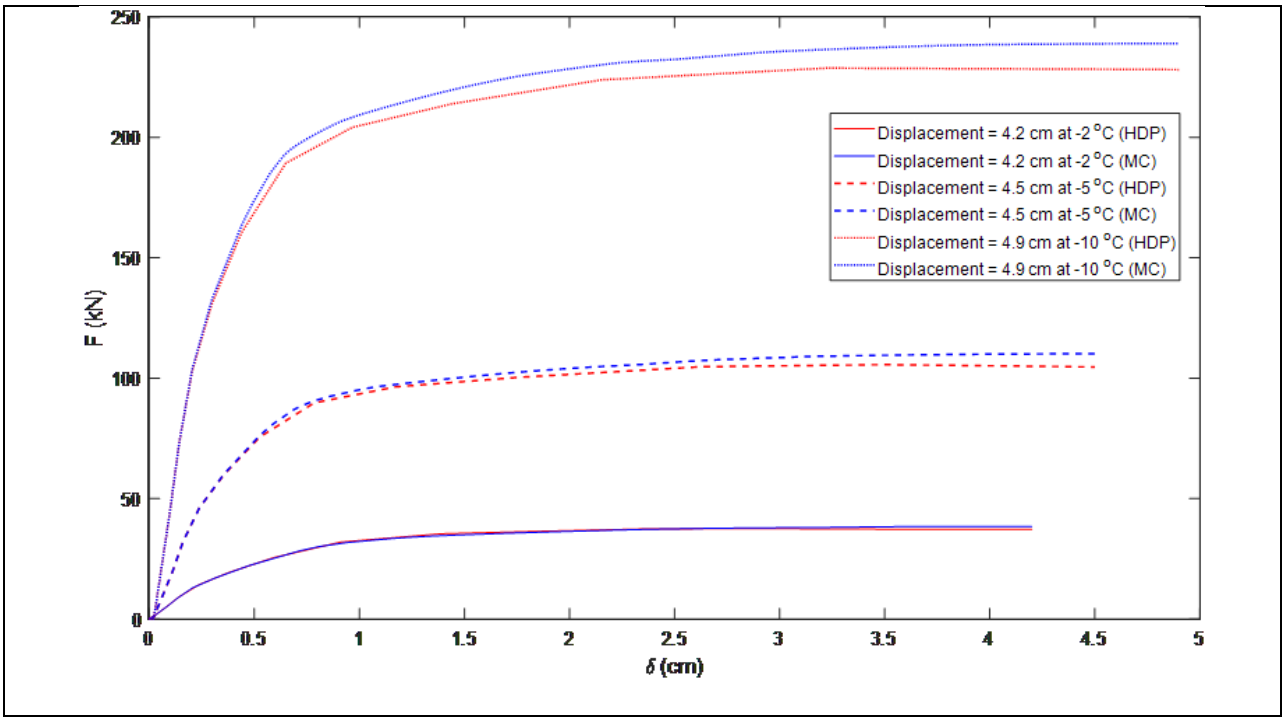

Figure 4. 6 Simulated uplift force-displacement relation for the buried pipe using different models (MCR = Mohr-Coulomb model with Rankine tensile cut-off, HDP = Hyperbolic Drucker-Prager).

The average equivalent plastic strain (ε^{pl}) distribution contours in the pipeline are shown in Figure 4.7 to Figure 4.9 at various displacements of the pipe. The equivalent plastic strain in soil body is increasing with an increase of uplift movement of pipe required for the failure of frozen soil with the drop of temperature and the maximum plastic equivalent strain is found at the soil present around the top edges of the pipe. The equivalent shear plastic strain (PEEQ) for shear yielding in Mohr-Coulomb criterion and the equivalent tensile plastic strain (PEEQT) for tensile yielding in Rankine criterion increase with the increases of uplift pipe displacement and a propagation of equivalent plastic strain with the increment of displacement can be visualized.

As is shown in Figures 4.7 - Figure 4.12, the produced plastic strain intensity is higher for the Mohr-Coulomb criterion as compared to Hyperbolic Drucker-Prager model at the same uplift vertical displacement of the pipe. In Hyperbolic Drucker-Prager model, tensile strength parameter is already considered in the criterion function, but in case of Mohr-Coulomb criterion, we must use Rankine tensile cut-off to consider the brittle behavior of frozen soil to analyze the failure behavior more precisely. Therefore, Abaqus gives tensile equivalent plastic strain (PEEQT) as it provides the option for tensile cut-off input parameters.

From the contours of these figures, the tensile strain has been developing at the mid-height of the pipe and propagate more inside, the output visualization contours are in aligned with the experimental results by Nixon (1998) and Liu et al. (2004). However, as it has been determined in chapter 3, strength parameters values increase with the decrease in temperature which leads to higher resistance. Thus, the uplift displacement is increased with the decrease in temperature to bring the pipeline to the failure stage but ends up with a higher uplift resistant force.

MCR-PEEQ MCR-PEEQT HDP-PEEQ

$\delta = 0.5$ cm

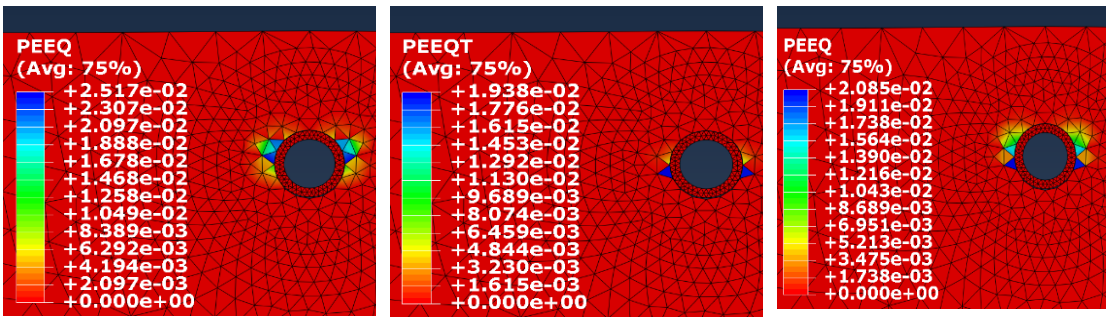

$\delta = 1$ cm

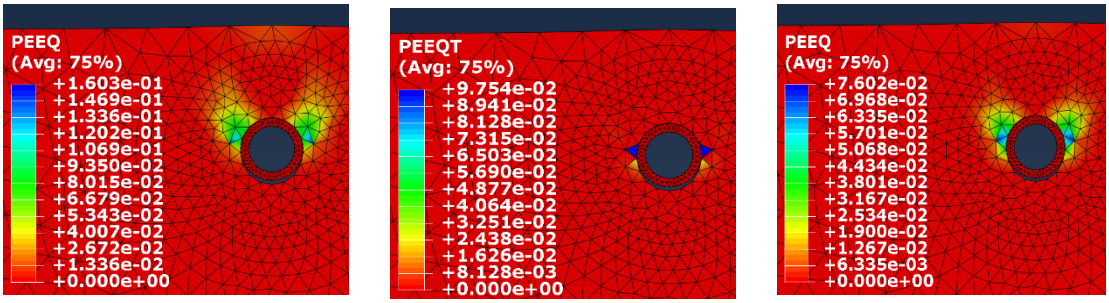

$\delta = 4$ cm

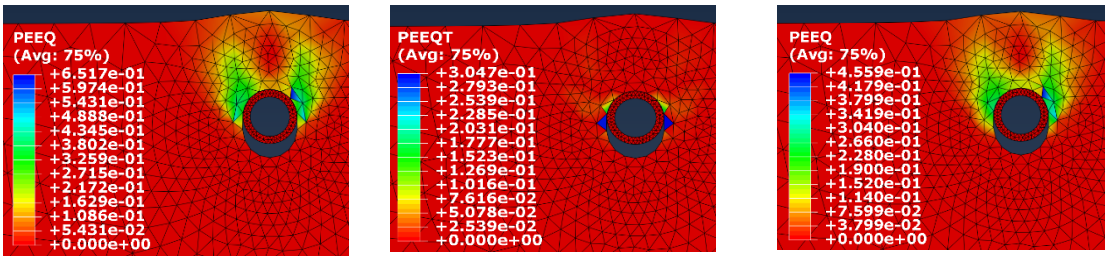

Figure 4. 7 Contour of the plastic strains at – 2 ºC.

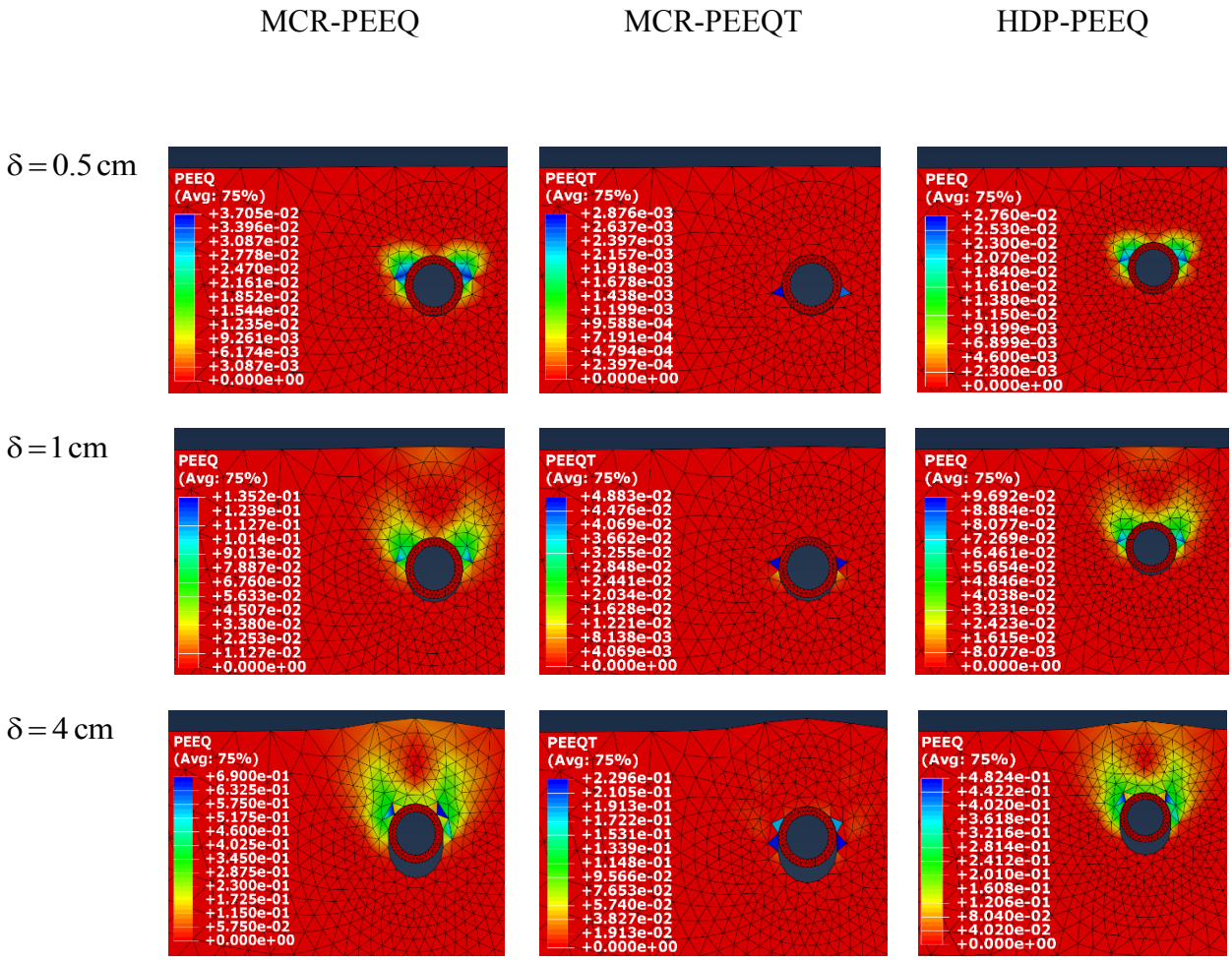

Figure 4. 8 Contour of the plastic strains at – 5 ^{o}C.

$\delta = 0.5\,cm$

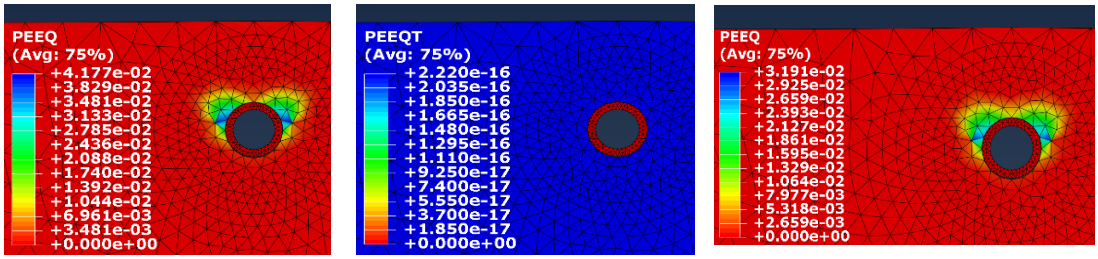

$\delta = 1\,cm$

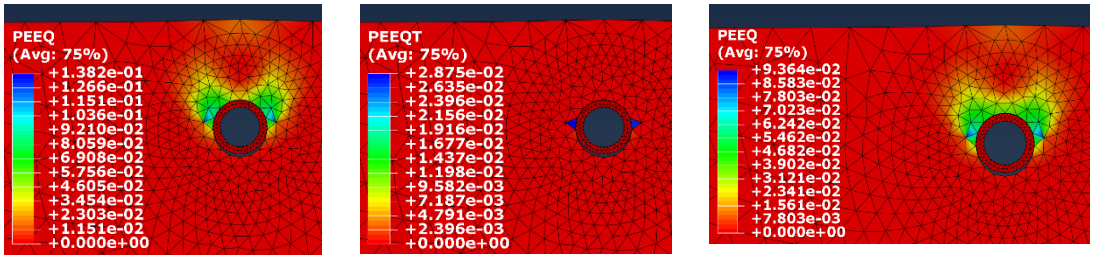

$\delta = 4\,cm$

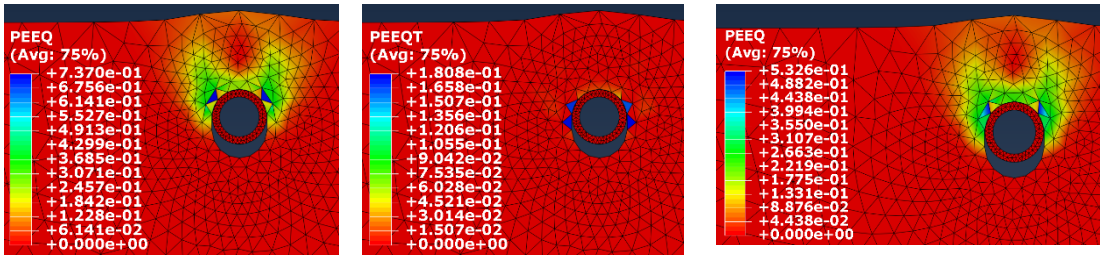

Figure 4. 9 Contour of the plastic strains at – 10 ºC.

4.3.3 Stress path analysis

As discussed in previous sections based on results, Neto et al. (2008) illustrated the possible matches between the family of Drucker-Prager model in various condition with the Mohr-Coulomb model as shown in Figure 3.7 and concluded that Drucker-Prager inscribed circle is the best fit for Mohr-Coulomb hexagon in-plane strain condition. In our theoretical approach and numerical model analysis, the hyperbolic Drucker-Prager circle inscribed the Mohr-Coulomb hexagon. The schematic view of MCR and HDP in the principal stress plane is given the Figure 4.10, which indicates that the HDP model should give more conservative results as compared to the MCR model.

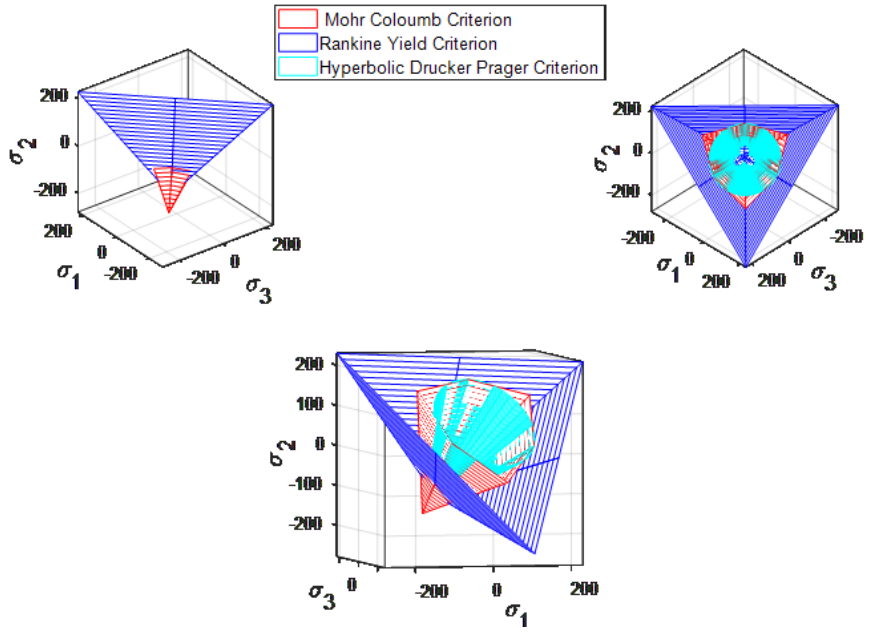

Figure 4. 10 Yield surfaces of the hyperbolic Drucker-Prager model and Mohr-Coulomb model with Rankine cut-off in the principal stress space.

Frozen soil at low temperatures acts like soft rocks, which leads it to a stronger compression and tension strength. A failure by compressive stresses cause a ductile failure which can be analyzed appreciatively by the Mohr-Coulomb but the failure pattern in the tensile stress is brittle, which is not that sharply applied in Mohr-Coulomb criterion, so Rankine maximum tensile cut-off surface is used to cover that brittle behavior. To avoid, the complication regarding Lode angle θ during the mathematical analysis, Hyperbolic Drucker-Prager is developed for the smooth circular surface, which not only counters the complexity of calculation for angle θ but also covers the sharp tensile strength behavior by considering the tensile strength parameter in its function.

The stress path followed by all four considered monitoring points (1,2,3,4) are shown in Figure 4.11a, b, and c and Figure 4.12a, b, and c for frozen soil at temperature - 2 ^{o}C, - 5 ^{o}C and - 10 ^{o}C respectively using both the Mohr-Coulomb with Rankine tensile cut-off (MCR) and hyperbolic Drucker-Prager (HDP) model.

Principal stress paths plot of the four monitoring points in the 3D space of principal stresses by Mohr-Coulomb with Rankine maximum tensile function and Hyperbolic Drucker-Prager function are given in Figure 4.11a, b, and c at - 2 ^{o}C, - 5 ^{o}C and - 10 ^{o}C, respectively. It is clear from these plots, Point (1) and Point (4) fails in the tension zone while point (2) and Point (4) touches the failure line in the shear zone. The principal stress path and the failure surface at different temperatures highlight that the hyperbolic Drucker-Prager failure criterion is more conservative towards tensile analysis of frozen soils and the smooth curve of the hyperbolic Drucker-Prager model make it easier to use during theoretical numerical modeling. The principal

stress path followed by these monitoring points also gives lower bound of strength in HPD as compared to MCR. Based on these outcomes, in this research, our prime consideration of selecting failure criterion will be the hyperbolic Drucker-Prager.

From Figure 4.12a, b, and c, the point (1), which is near the top of the soil block at the vertical position of pipe, fails in tension by touching the failure line in tension zone showing increasing resistance towards tensile failure with decreasing temperature. Point (2), on the vertical front surface of soil just above the pipe, fails by touching the failure line in the shear zone, because of the compression produced due to pipe uplifting but the shearing behavior of frozen soil becomes more prevailing with the decreasing of temperature. This point also presents the increasing crushing behavior with the decrease of temperature. At low frozen temperature, after touching failure line in the shear zone, stress path yields towards tensile zone while at high frozen temperature, it remains in the shear failure zone. Point (3), is near the left spring line of the pipe, shows a minor tensile behavior and then enter a shear zone where it touches the failure line and this behavior becomes abrupt with respect to the temperature drop. This shear zone was also identified in the work of Liu et al. (2004). Point (4), which is at the left upper portion of the pipe's spring line, shows a failure in the tensile zone with a little initial shear strength but at – 10 ^{o}C temperature, a minor shear behavior is encountered as compared to higher temperatures.

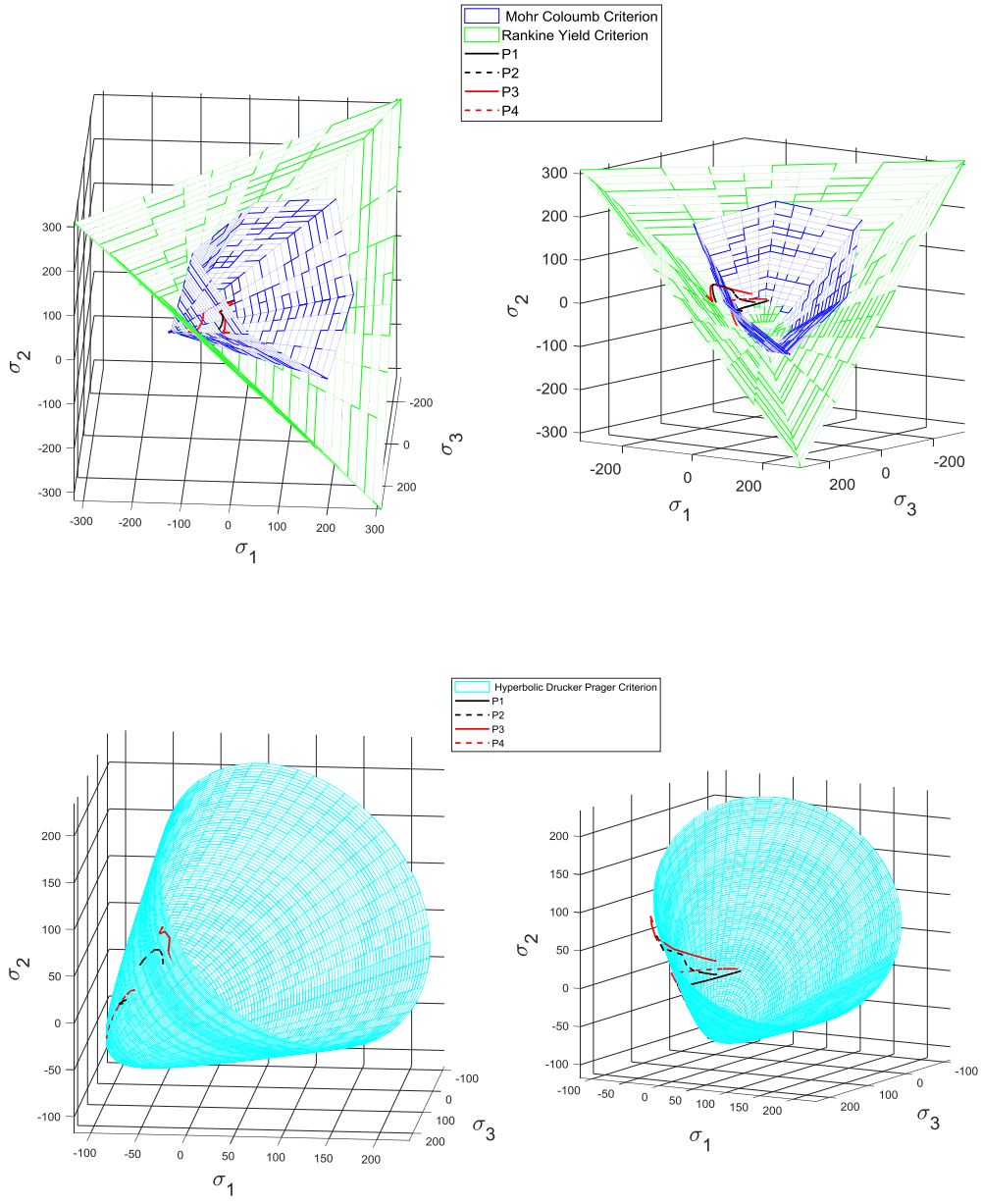
Mohr Coloumb Criterion
Rankine Yield Criterion
P1
P2
P3
P4
σ1
σ2
σ3
Hyperbolic Drucker Prager Criterion
P1
P2
P3
P4
σ1
σ2
σ3

(a) T = -2 ºC

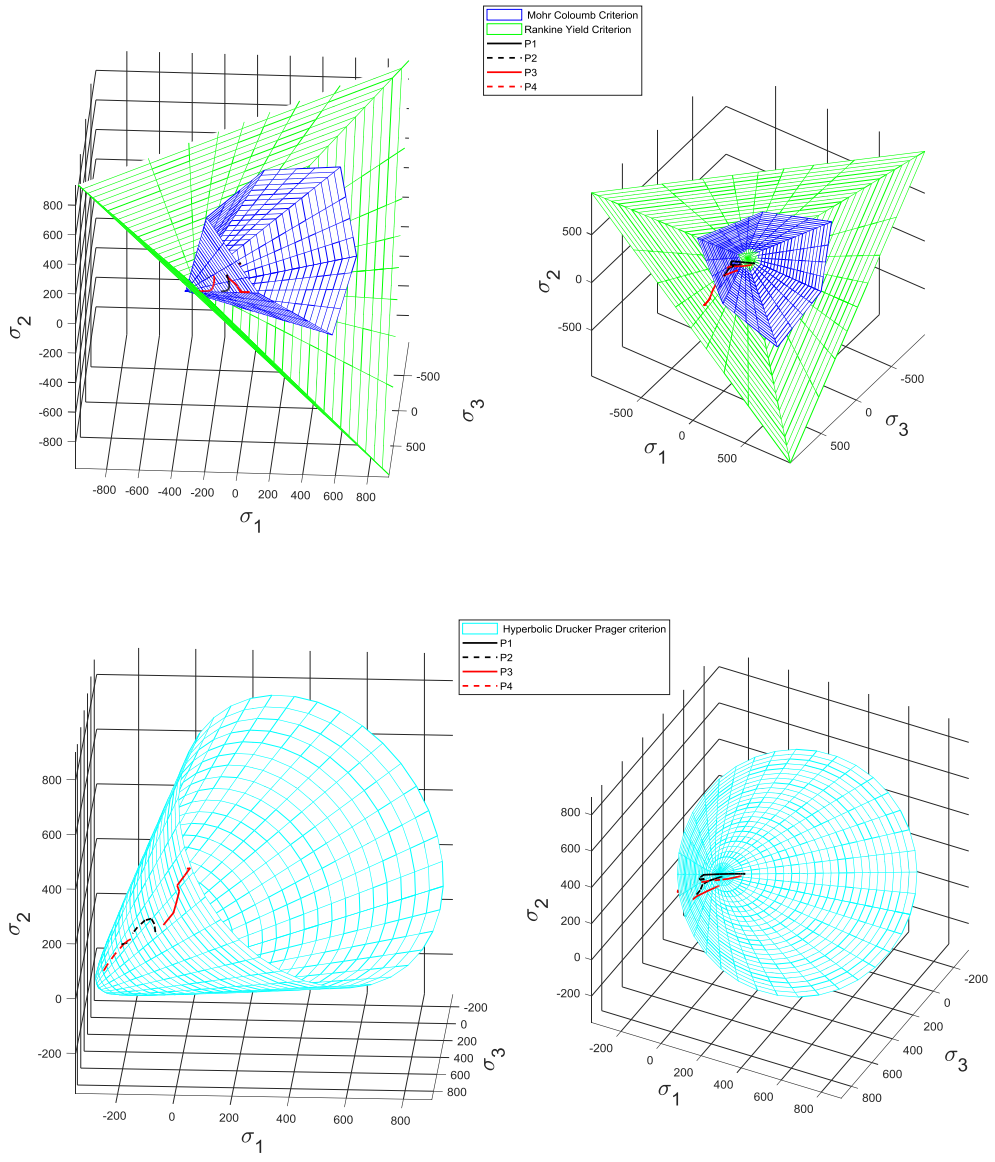
Mohr Coloumb Criterion
Rankine Yield Criterion
P1
P2
P3
P4
σ1
σ2
σ3
Hyperbolic Drucker Prager criterion
P1
P2
P3
P4
σ1
σ2
σ3

(b) T = -5 ^{o}C

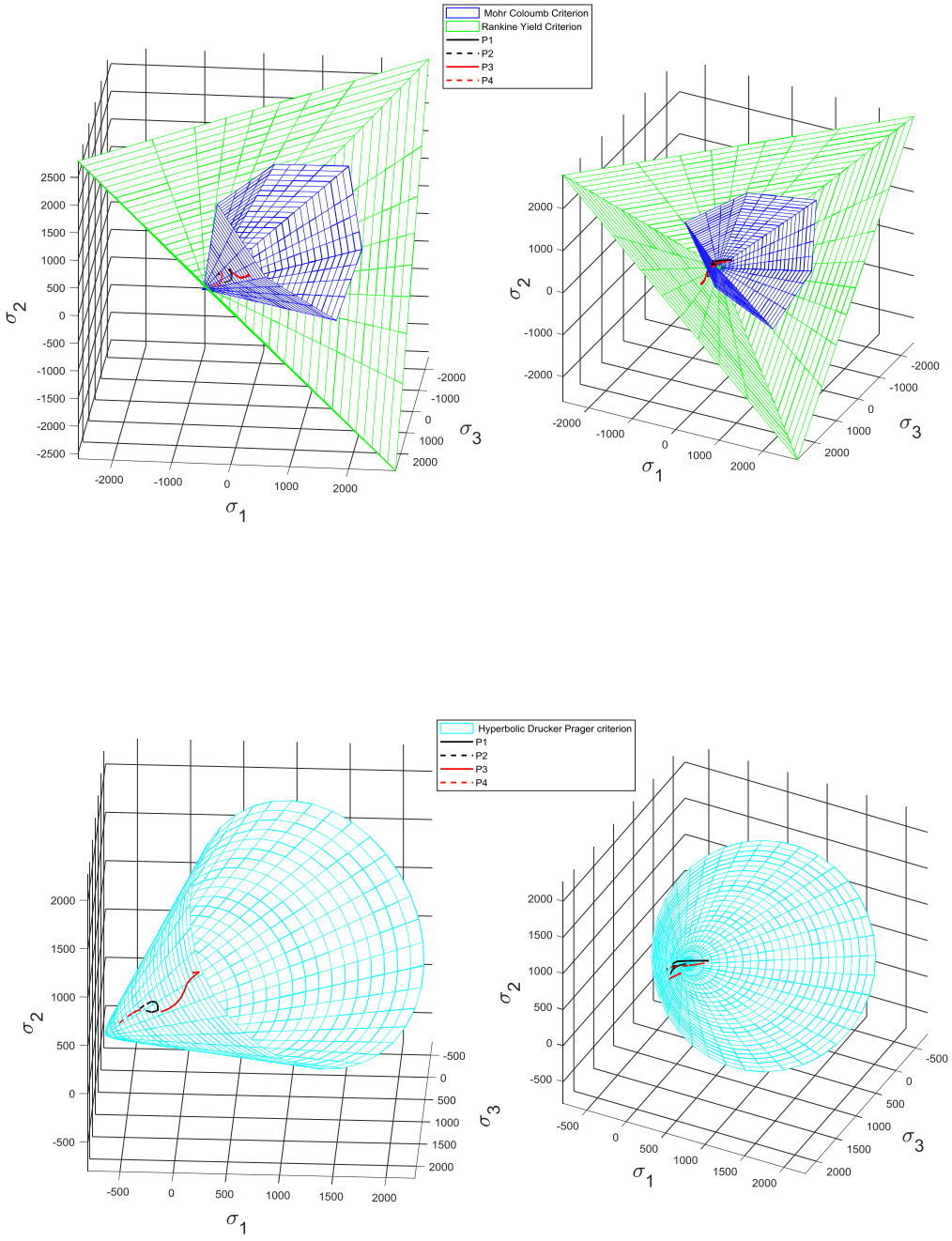

(c) T = -10 °C

Figure 4. 11 Stress path of four monitoring points for the frozen clay pipe interaction analysis in principal stress space at different temperatures.

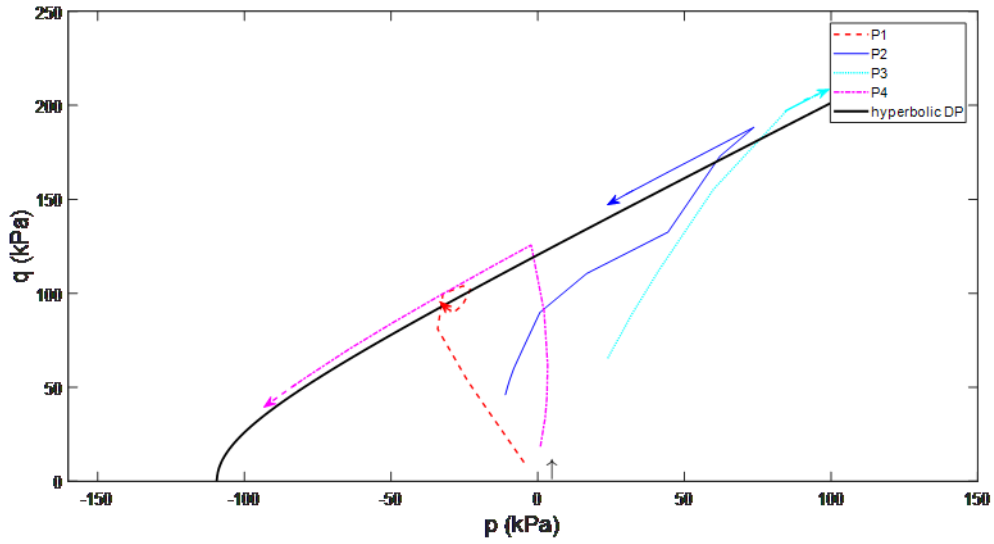
P1
P2
P3
P4
hyperbolic DP
q (kPa)
p (kPa)
250
200
150
100
50
0
-150
-100
-50
0
50
100
150

(a) T = - 2 ºC

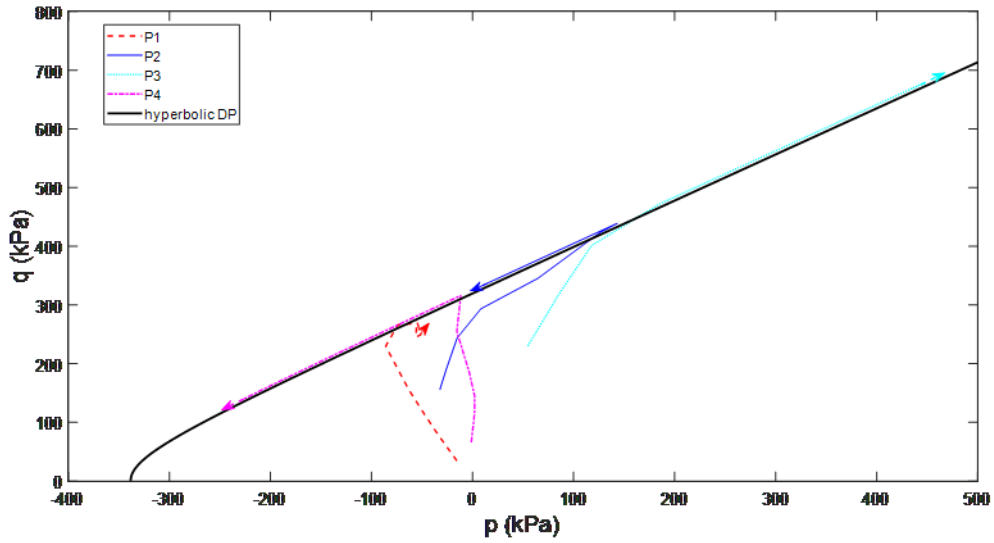
P1
P2
P3
P4
hyperbolic DP
q (kPa)
p (kPa)
800
700
600
500
400
300
200
100
0
-400
-300
-200
-100
0
100
200
300
400
500

(b) T = - 5 ºC

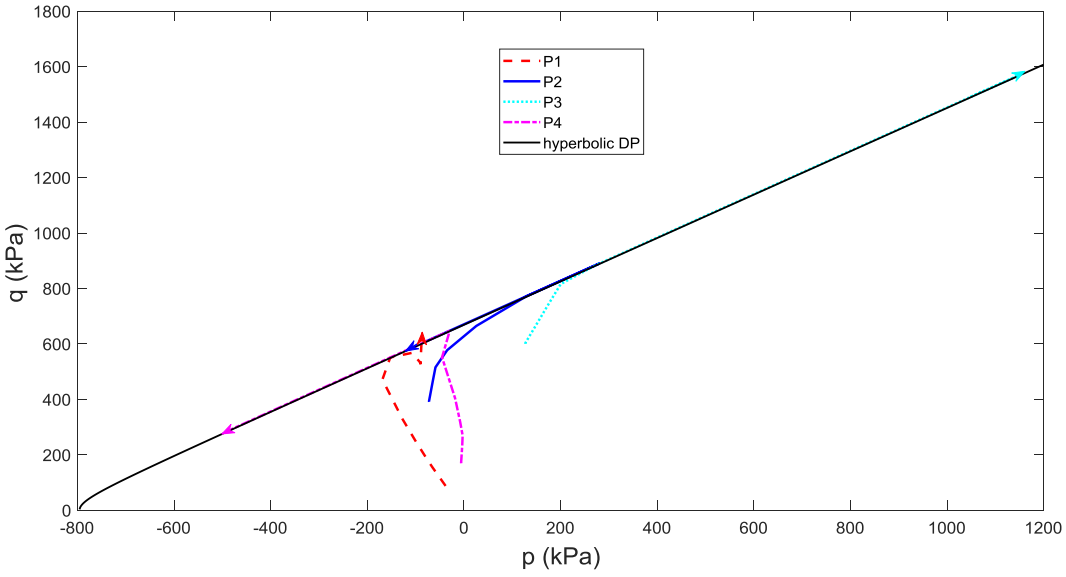

(c) T = - 10 ºC

Figure 4. 12 Stress paths of four points for the frozen clay pipe interaction analysis in mean effective force (p) and equivalent deviatoric stress (q) plane at different temperatures.

4.4 FEM analysis of soil-pipe interactions at transient frozen temperatures

Soil-pipe interactions at transient frozen temperatures were performed to study the effect of thermal variation in a frozen soil under a constant uplift force condition. Firstly, soil matrix was kept at –15ºC which is in the predefined field available in Abaqus, then in the first Geo-static step, gravitational forces were introduced into the soil followed by gravity in the pipe in static general step and a vertical upward force was applied through a pipe in the third step.

Subsequently, the temperature at soil pipe interface was increased to -2°C while the outer boundaries of soil block were kept at -15°C during the step of coupled thermal-mechanical analysis for 24 hours. In this group of numerical simulation, only the hyperbolic Drucker-Prager model is applied.

4.4.1 Heat transfer analysis

The variation in the thermal energy with respect to time in a frozen soil block is shown in Figure 4.13a, b, c, and d after 2, 6, 12, and 24 hours. The temperature variation in all four monitoring points of frozen soil is given in Figure 4.14. It can be illustrated that from above-mentioned figures for monitoring points that it may take less than 24 hours for this frozen soil mass, depends on thermal properties, to reach fully thermal steady stage but the point, which is under consideration for analysis purposes, has already reached a steady state of temperature just after 7 hours as can be seen in Figure 4.14. Point (1), which is near the top surface of soil and far from pipe, temperature of this point increase to -13°C and become steady while the point (3) and point (4) are being near to pipe, their temperature increased to maximum steady stage of – 4 °C and – 6 °C respectively.

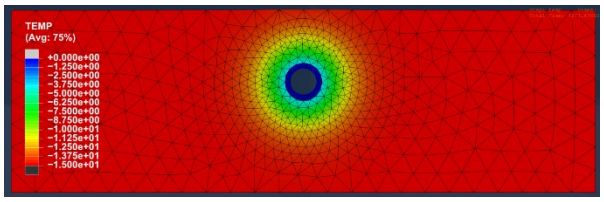

(a) t = 2 hours

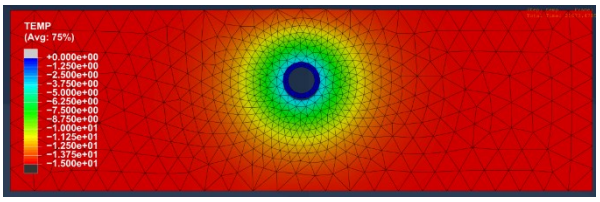

(b) t = 6 hours

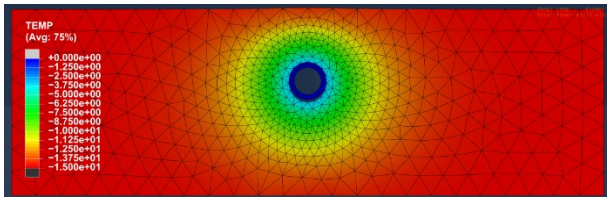

(c) t = 12 hours

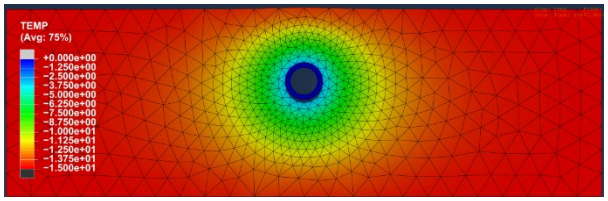

(d) t = 24 hours

Figure 4. 13 Variation of temperature in frozen soil with respect to time

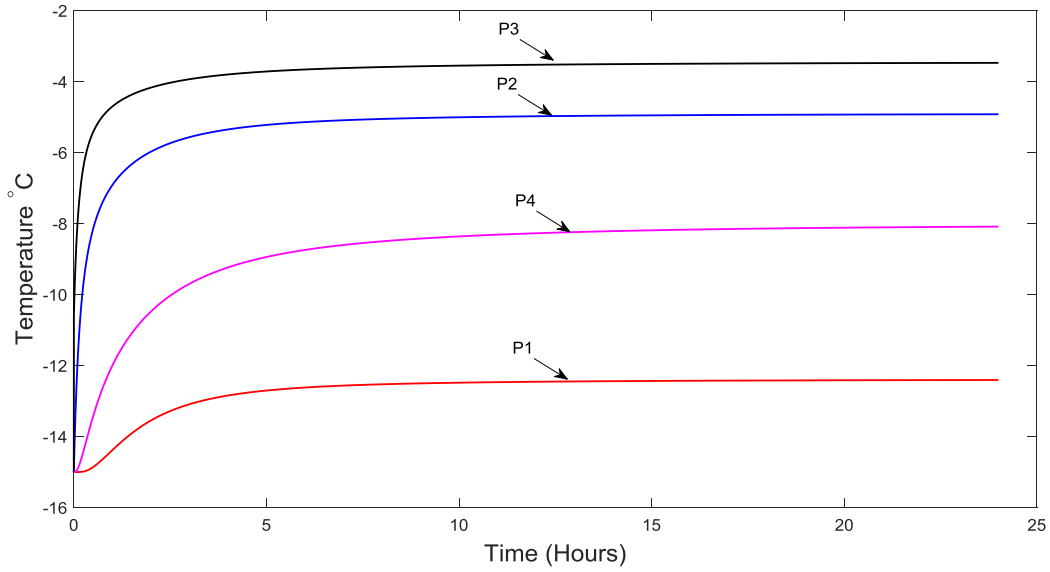

Figure 4. 14 Plot of the temperature variation in selected four monitoring points with respect to time.

4.4.2 Uplift resistance and plastic strain

Different vertical uplift forces were applied through a pipe in the frozen soil and kept constant during the transient heat transfer process to study the failure pattern using the hyperbolic Drucker-Prager model. By the end of the numerical tests, results of vertical uplift displacements contours are given in Figure 4.15a, b, and c for the cases of the total vertical force of 24.6 kN, 123 kN, and 184.5 kN respectively.

The displacement variation in a soil matrix shows that it is dependent on applied vertical forces and on temperature variations as the soil mechanical strength parameters change drastically with frozen temperature discussed in detail in Chapter 3. The frozen soil near the vertical top of the pipe has a larger displacement as compared to the soil away from the pipe. The displacement of pipe in a frozen soil also increases with the applied vertical load, the total vertical forces 24.6 kN, 123 KN, and 184.5 kN cause maximum displacement of around 0.00127 m, 0.005 m, and 0.012 m respectively.

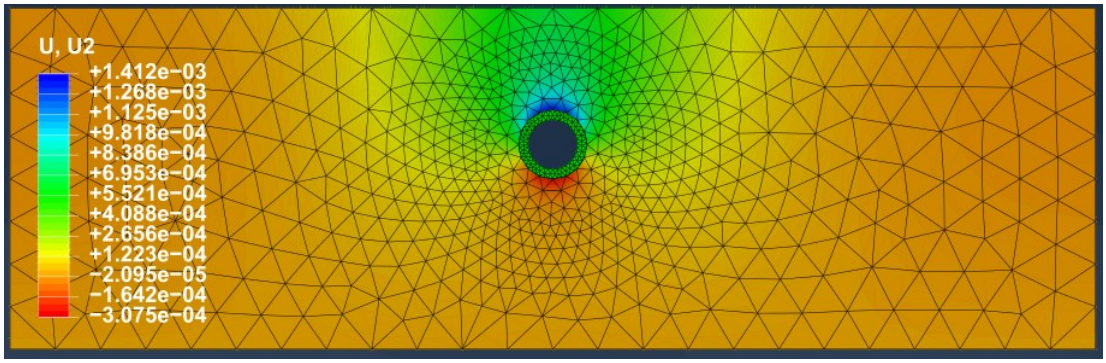

(a) F = 24.6 kN

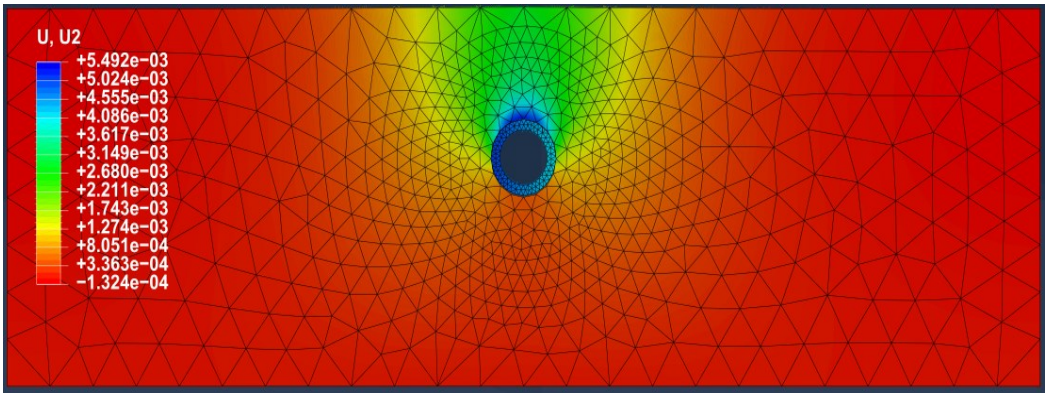

(b) F = 123 kN

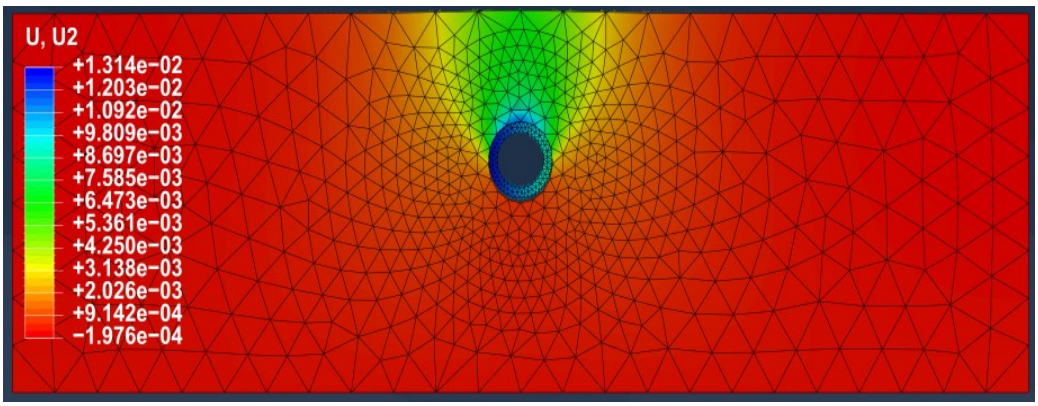

(c) F = 184.5 kN

Figure 4. 15 Contour plot of uplift vertical displacement (U2) due to temperature change at different constant vertical forces, t = 24 hours.

Plots of normal resistant force with respect to vertical displacement during mechanical and thermal loading conditions are shown in Figure 4.16. When the vertical force of 24.6 kN is applied in a pipe, normal reaction force linearly increases with the displacement of pipe, and then shows a suddenly small drop in strength followed by an increase in the normal reaction. This behavior is because of the induced thermal energy which significantly reduced the mechanical strength by increasing the temperature of soil mass elements and at the end showing strength recovery because of the steady state achieved by the soil element. A similar pattern can be witnessed when 123 kN and 184.5 kN total vertical forces were applied in the pipe to produce uplift displacement as normal reaction force increases with the displacement linearly followed by a drop in normal force. The total vertical force of 184.5 kN by pipe gives a linear response of resistance force with uplift displacement, followed by the straight horizontal line, showing no increase in normal force which is a sign of failure phase in the soil block of the pipeline.

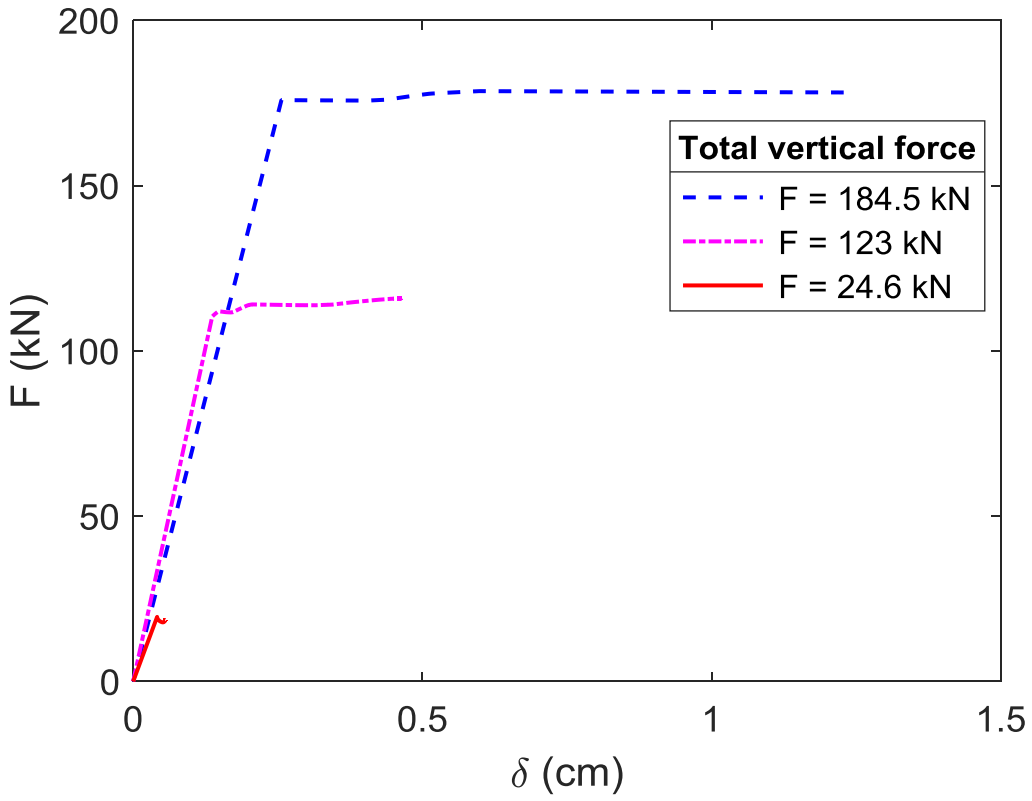

Figure 4. 16 Plot of normal resistant force with respect to vertical displacement during mechanical and thermal loading conditions.

Equivalent plastic strain (ε^{pl}) is a scalar form of plastic strain (PE). It depends on the permanent uplift displacement of pipe and it is also affected by the temperature-dependent mechanical strength parameters of frozen soils. Figure 4.17 presents the variation of plastic strain in the frozen soil around the pipe. Figure 4.20a with low applied vertical force shows minor plastic strain around the pipe where small plastic strain due to gravity pull of pipe can also be visualized due to the increase in temperature. The increase in the plastic strain in the soil matrix with the increase of applied vertical force due to transient heat transfer in the matrix is shown in the Figures 4.20a, b, and c, where plastic strain produced at the nearest layer of soil around the pipe and propagate inside the soil matrix with the increase of thermal induction.

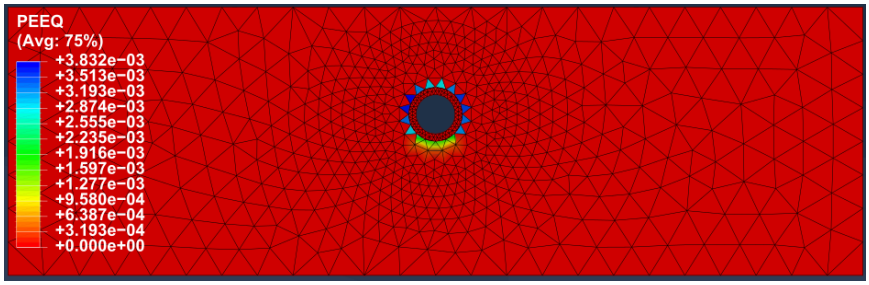

(a) F = 24.6 kN

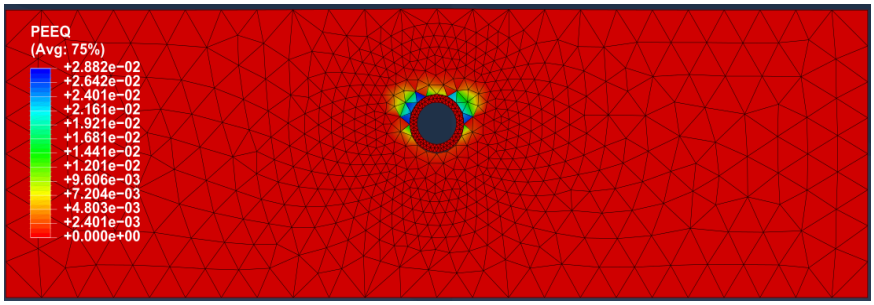

(b) F = 123 kN

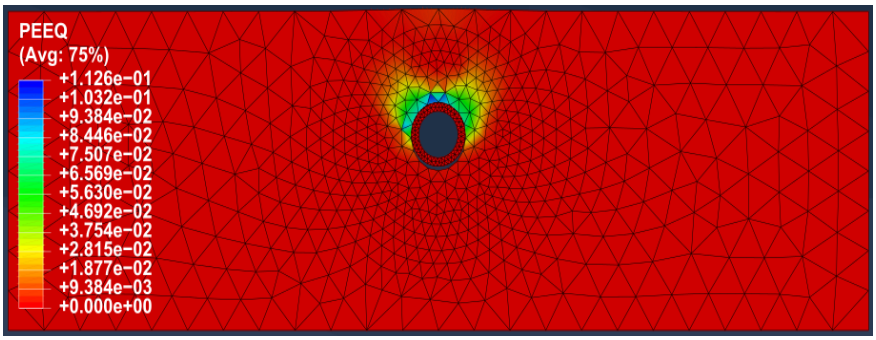

(c) F = 184.5 kN

Figure 4. 17 Contour plot of Equivalent Plastic Strain (PEEQ) due to temperature change at different constant vertical uplift forces, t = 24 hours.

4.4.3 Stress path analysis

The frozen clay soil has a higher strength at –15ºC as compared to - 2ºC, so a change in thermal state of frozen soil will drastically disturb the bearing strength of the frozen soil as shown in Figure 4.18a, b, and c. The stress paths for cases with thermal transfer processes are complicated. The stress paths of monitoring points (2) and (3) at a constant applied uplift force, tend to touch the yield surface of - 7ºC when the temperature of soil pipe interface increases from –15ºC to –2ºC. The stress paths of points (1) and (4) show some resilient towards failure line produced at -7ºC as the temperature at these points after 24 hours are -8ºC and -13ºC.

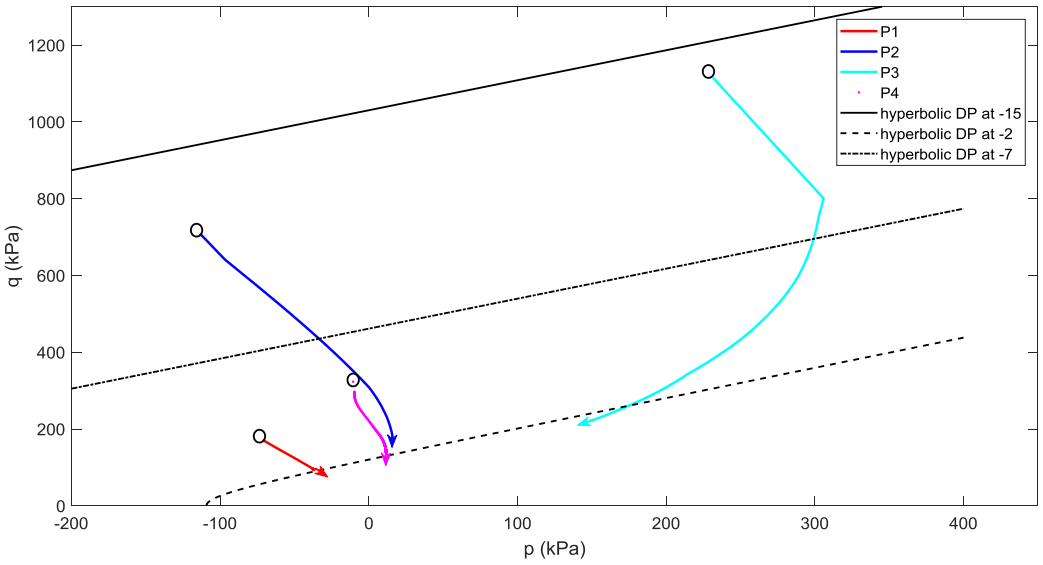

(a) F = 24.6 kN

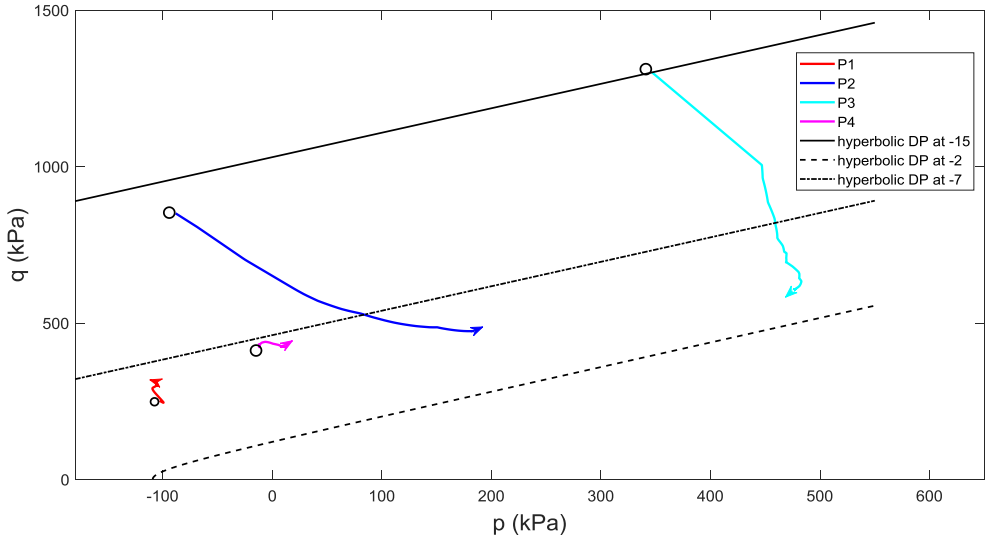

(b) F = 123 kN

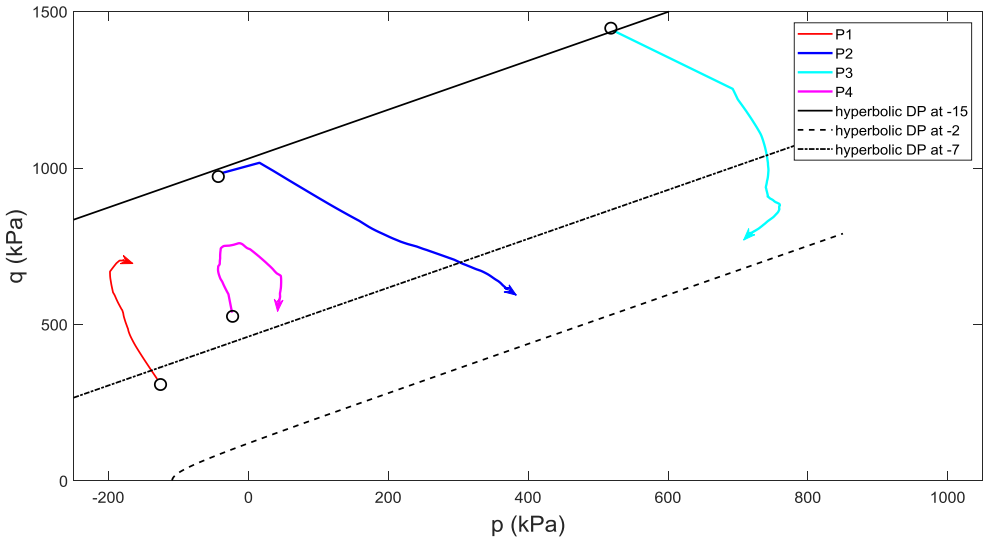

(c) F = 184.5 kN

Figure 4. 18 Stress path plot of monitoring points in mean effective Force (p) and Equivalent deviatoric stress (q) plane due to temperature change at different constant vertical uplift forces, t = 24 hours.

4.5 Summary

The frozen clay shows more reaction or resistance towards the uplift displacement with respect to a lower temperature. The lower the temperature the higher the resistance force and a larger displacement of pipe will be required to create failures in the frozen soil. Under a plane-strain condition, the numerical simulation results show that the hyperbolic Drucker-Prager model gives more conservative results as compared to the Mohr-Coulomb model with Rankine cut-off. Thermally induced plastic strain in frozen ground can be characterized using an explicit way where the yield surface is drifted with an increase of temperature.

CHAPTER 5

CONCLUSION AND RECOMMENDATION FOR FUTURE WORK

5.1 Summary of thesis contributions and conclusions

Temperature-dependent mechanical properties of a frozen clay:

- The mechanical strength of frozen soil (e.g. Young's modulus, Poisson's ratio, cohesive strength, tensile strength, and uniaxial compression strength) is both frozen temperature and strain rate dependent. At higher frozen temperature (below -5 ^{o}C), a linear relationship exists between temperature and strength parameters. And the higher strain rate leads to higher values of strength parameters while lower strain rate yields lower values for strength parameters
- At lower frozen temperature (between 0 ^{o}C and - 5 ^{o}C) in case of the warm-frozen condition of the soil, the non-linear relationship defined by power law equation ($X = AY^{B}$) relates temperature and strength parameters.
- The change of unfrozen water content to frozen water content of frozen soil (clays and silts) is optimum at - 5 ^{o}C, after which the available unfrozen water content will no more be affected by the temperature drop.
- The complex behavior of frozen soil is because of frozen water content, which plays a vital role in increasing the cohesive strength of frozen soil because of sticky and adhesive nature.

Frozen soil-pipe interaction at constant frozen temperatures:

- During uplift displacement of pipe in the soil matrix, tensile cracks produce near each spring line of the pipe and propagate inside the soil matrix away from the pipe. One tensile crack also appeared at the top surface of soil above the pipe and propagate inside the soil matrix towards the pipe.
- The uplift resistance in terms of bearing capacity increases with the decrease of temperature because of temperature-dependent mechanical strength parameters. The need for uplift displacement increases from 4.2 cm to 4.9 cm to bring the soil to failure when the frozen temperature increases from - 2 ^{o}C to -10 ^{o}C. The reaction force also increases from 38.45 kN to 238.9 kN in MCR model and 37.24 kN to 228.1 kN in HDP model when the frozen temperature increases from - 2 ^{o}C to -10 ^{o}C.
- Plastic strain develops near the spring line of pipe and increases with the uplift displacement and propagate inside the soil matrix following the path of pipe movement.
- The monitoring points in the frozen soil matrix near the pipe (e.g. Point (2) and (3)) between the spring line and vertical surface pipe position shows a shear failure while the monitoring points (e.g. Point (1) and (4)) lying away from pipe shows a trend of tensile failure. Points show more crushing behavior at lower temperature acting like soft rock.

Frozen soil-pipe interaction in transient heat state:

- The bearing capacity (uplift resistance) in terms of normal reaction force reaches to peak curve for frozen soil with respect to uplift vertical force at a highest frozen temperature and becomes straight horizontal line giving failure stage because of thermal induction in the frozen soil. The transition zone during heat transfer stage causes a minor drop in the bearing capacity and becomes stable once the steady stage for temperature reached. At a vertical uplift force, 184.5 kN by pipe gives the maximum value of resistance force of 178.2 kN.
- Temperature-dependent mechanical strength plays a vital role during transient heat transfer stage. A premature complex failure stage occurs during the heat transfer inside the soil matrix at a constant upward vertical force which may lead to the drastic failure situation. A considerable loss in tensile and shear strength of frozen soil is visualized with the decrease of temperature.

Comparative failure analysis based on Mohr-Coulomb with Rankine tensile cut-off criterion and Hyperbolic Drucker-Prager criterion:

- Frozen soil behaves like soft rocks show a brittle tensile failure which may not be captured in Mohr-Coulomb criterion make it necessary to use the Rankine maximum tensile cut-off criterion along with it.
- Hyperbolic Drucker-Prager criterion use integrated tensile parameter in the yield function which yields upper bound values for uplift displacement and gives lower bound values for bearing capacity (e.g. 229.7 kN as compared to

238.9 kN of MCR). This property makes it more conservative to be used in the analysis of brittle tensile failures conditions.

- During a plane strain approach of failure analyses, the hyperbolic Drucker-Prager yields a smooth inscribed circle to the Mohr-Coulomb hexagon in a principal stress plane, which makes the calculation required for determination of θ easy and effective.

5.2 Recommendation for future work

To achieve the required amount of strength of soil for transportation purposes like deep tunnel passing though marine area having very soft soil, using pipe transportation system for transporting natural resources, bring also a lot of serious concerns regarding the short-term and long-term sustainability of structures. Thus, the behavior of permafrost soil or artificially frozen soil should be studied further in details for the benefit of mankind. The following recommendations are made for future work:

- More field and laboratory tests at various transient expected temperatures are recommended to be performed to investigate the real-field interactions between the frozen soil and pipes.
- Temperature-dependent mechanical strength properties are needing to be determined during warm- frozen condition while the temperature varies from + 4 ^{o}C to – 10 ^{o}C, to investigate the nonlinearity effect because of available water content.
- Laboratory experiments need to be performed to investigate an elastoplastic strain hardening and flow rule behavior of frozen soil.

- Horizontal stress produced in pipes during flow along with longitudinal vertical displacement should be studied in detail using both laboratory investigations and numerical simulations.
- Brittle fracture failure approach during landslides or earthquakes should be studied in detail, as it could be the biggest issue in the areas which have fault lines and this study can be done through both laboratory demonstration and simulation techniques.
- The behavior of warm frozen soil should be studied with the consideration of phase change. Theories in micromechanics and thermodynamics should be applied to figure out the large strain behavior of frozen soil when the applied temperature and stress condition cause melts. The failure pattern of soils and the displacement of pipes should bear with a very different behavior when the phase change of ice in frozen soil is considered.

REFERENCES

Abaqus. (2014). Abaqus theory manual, Version 6.14. Simulia.

Azmatch, T.F., Sego, D.C., Arenson, L.U., & Kevin, W.B. (2011). "Tensile Strength and Stress-Strain Behaviour of Devon Silt under Frozen Fringe Conditions." *Cold Regions Science and Technology 68*(1–2):85–90.

Azmatch, T.F., Sego, D.C., Arenson, L.U., & Kevin, W.B. (2010). "Tensile Strength of Frozen Soils Using Four-Point Bending Test." *63rd Canadian Geotechnical Conference & 6th Canadian Permafrost Conference* 436–42.

Bolton, M. D. (1986). "The Strength and Dilatancy of Sands." *Geotechnique 36*(1):65–78.

Casamichele, P., Maugeri, M. & Motta, E. (2004). "Non-Linear Analysis of Soil-Pipeline Interaction in Unstable Slopes." *13th World Conference on Earthquake Engineering, Vancouver, Canada*.

Chan, P.D.S & Wong, R.C.K. (2004). "Performance Evaluation of a Buried Steel Pipe in a Moving Slope: A Case Study." *Canadian Geotechnical Journal 41*(5):894–907.

Chen, W.F. & Han, D.J. (1989). *Plasticity for Structural Engineers*.Springer-Verlag, New York

Chen, Y., Azzam, R., Wang, M., Xu, S., & Chang, L. (2011). "The Uniaxial Compressive and Tensile Tests of Frozen Saturated Clay in Shanghai Area." *Environmental Earth Sciences 64*(1):29–36.

De Souza Neto, E. A., Peric, D., & Owen, D. R. J. (2008). Computational Methods for Plasticity: Theory and Applications. Wiley, New York.

Esmaeili-Falak, M., Katebi,H., & Javadi,A. (2018). "Experimental Study of the Mechanical Behavior of Frozen Soils - A Case Study of Tabriz Subway." *Periodica Polytechnica Civil Engineering 62*(1):117–25. https://doi.org/10.3311/PPci.10960

Fjær, E., P. Horsrud, Holt, R.M., Raaen, A.M., & Risnes, R. (2008). *Petroleum Related Rock Mechanics*(2nd ed.). Elsevier Science.

Foriero, A. & Ladanyi, B. (1994). "Pipe Uplift Resistance in Frozen Soil and Comparison with Measurements." *Journal of Cold Regions Engineering 8*(3):93–111.

Guo, P. (2005). "Numerical Modeling of Pipe–Soil Interaction under Oblique Loading." *Journal of Geotechnical and Geoenvironmental Engineering 131*(2):260–68.

Guoqing, Z., Hu, K., Wang, J., Liang, H., & Lu, G. (2015). "Laboratory Investigation on Tensile Strength Characteristics of Warm Frozen Soils." *Cold Regions Science and Technology 113*(2015):81–90.

Hikooei, B.F. (2013). "Numerical Modeling of Pipe Soil Interaction under Transverse Direction." M.Sc. Thesis, Department of Civil Engineering, University of Calgary. Calgary, Alberta, Canada.

Jung, J.K., O'Rourke,T.D., & Olson, N.A. (2013). "Lateral Soil-Pipe Interaction in Dry and Partially Saturated Sand." *Journal of Geotechnical and Geoenvironmental Engineering 139*(12):2028–36.

Kouretzis, G.P., Krabbenhøft, K., Sheng, D., & Sloan, S.W. (2014). Soil-buried pipeline interaction for vertical downwards relative offset. Canadian Geotechnical Journal, 51(10): 1087–94. doi:10.1139/cgj-2014-0029.

Leung, R. K. Y., Ko,. K. Y., Hu, H.B., Cheung, A.K.K., & Chan, W.L. (2012). "Artificial Ground Freezing for Tbm Break-Through – Design Considerations." *In Proceedings of the HKIE Geotechnical Division Annual Seminar* :119–24.

Li, B. & Wong, R.C.K. 2016. "Quantifying Structural States of Soft Mudrocks." *Journal of Geophysical Research: Solid Earth 121*(5):3324–47. doi:10.1002/ 2015JB012454.

Li, H.P., Zhu, Y.L., & Pan, W.D.(2003). "Uniaxial compressive strength of saturated frozen silt.'' *Permafrost, Phillips, M., Springman, S.M., and Arenson, L.U., Eds., Lisse: Swets and Zeitlinger*:679–684.

Liu, B.Y., Crooks, J.H.A., Nixon, J.F., & Zhou, J.Z., (2004a), "Experimental Studies of Pipeline Uplift Resistance in Frozen Ground", *IPC. Calgary, Canada*. (pp. 2407–13).

Liu, B.Y., Crooks, J.H.A., Nixon, J.F., & Zhou, J.Z., (2004b), "Numerical Studies of Pipeline Uplift Resistance in Frozen Ground", *IPC. Calgary, Canada*. (pp. 2423–28).

Merifield, R., White,D.J., & Randolph, M.F. (2008). "The Ultimate Undrained Resistance of Partially Embedded Pipelines." *Géotechnique 58*(6):461–70. https://doi.org/10.1680/geot.2008.58.6.461

Ming, F., Li, D., Zhang, M, & Zhang,Y. (2017). "A Novel Method for Estimating the Elastic Modulus of Frozen Soil." *Cold Regions Science and Technology 141*:1–7.

NEB. (2011). "Safety and Environment. (December). " *Retrieved from (http://www.ics -shipping.org/key-issues/safety-and-environment).*

NEB. (2012). "Technical Considerations : Implementing the Decision." 2:1–310. *Retrieved (https://www.neb-one.gc.ca/pplctnflng/mjrpp/archive/mcknzgs/rfd/rfdv2-eng.pdf).*

Nixon, J. F. (1991). "Discrete Ice Lens Theory for Frost Heave in Soils." *Canadian Geotechnical Journal 28*(6):843–59.

Nixon, J.F. (1998), "Pipe Uplift Resistance Testing in Frozen Soil", *Proceedings: 7th International Permafrost Conference. June.*

Nyman, K. J. (1984). "Soil response against oblique motion of pipes." *Journal of Transportation Engineering 110*(2):190–202.

O'Rourke, T. D. & Trautmann, C. H. (1985). "Lateral Force-Displacement of Buried Pipe Response." *Journal of Geotechnical Engineering 111*(9):1077–92.

PHMSA. (2018). Significant pipeline incidents. Retrieved from U.S. deparment of transportation: *Retrieved from (https://hip.phmsa.dot.gov/analyticsSOAP/saw.dll?Portalpages).*

Rajeev, P., & Kodikara, J. (2011). "Numerical Analysis of an Experimental Pipe Buried in Swelling Soil." *Computers and Geotechnics 38*(7):897–904. doi:10.1016/j.compgeo.2011.06.005.

Razaqpur, A.G., & Wang, D. (1996). Frost-induced deformations and stresses in pipelines. *International Journal of Pressure Vessels and Piping*, 69: 105–118.

Rosenfeld, M. J., PE, & Auker, M.V. (2012). "Distribution Pipeline System Integrity Threats Related to Cold Weather." *Kiefner & Associates, Inc.*

Scarpelli G., Sakellariadi E., & Furlani G. (2001). "Numerical Analysis of Soil-Pipeline Interaction Phenomena in Unstable Slopes." *XV ICSMFE, Proceedings of the Fifteenth International Conference on Soil Mechanics and Foundation Engineering* 1315–18.

Tokimatsu, K. & Seed, H.B. (1987). “Evaluation of Settlements in Sands.” *Journal of Geotechnical Engineering 113*(8):861–78.

Young-kyo, S & Heon-woo, C. (2012). “Experimental Study on Unconfined Compression Strength and Split Tensile Strength Properties in Relation to Freezing Temperature and Loading Rate of Frozen Soil.” *Journal of Ocean Engineering and Technology 26*(6):19–26. http://dx.doi.org/10.5574/KSOE.2012.26.6.019

Wong, C. K., Wan, R.G., Wong, R., & Liu, B.(2016). “Physical Modelling on Buried Pipeline Response in Elasto-Viscoplastic Soils.” *11th International Pipeline Conference* 1–9.

Xiang-dong, H., Jin-tai,W., & Rui-zhi, Y. (2013). “Uniaxial Compressive and Splitting Tensile Tests of Artificially Frozen Soils in Tunnel Construction of Hong Kong.” *Journal of Shanghai Jiaotong University (Science) 18*(6):688–92.

Xiao-dong, Z., Guo-qing, Z., Wei,C., & Xiao-jun, L. (2009). “Effects of Temperature Gradients on Elastic Modulus and Compression Strength of the Saturated Frozen Clay.” *Procedia Earth and Planetary Science* 1(1):420–24. https://doi.org/10.1016/j.proeps.2009.09.067.

Xu, X., Wang, Y., Yin, Z., & Zhang, H. (2017). “Effect of Temperature and Strain Rate on Mechanical Characteristics and Constitutive Model of Frozen Helin Loess.” *Cold Regions Science and Technology* 136:44–51.

Yin, J-H. (1999). “Properties and Behaviour of Hong Kong Marine Deposits with Different Clay Contents.” *Canadian Geotechnical Journal 36*(6):1085–95.

Yin, J-H. (2001). “Stress-Strain-Strength Characteristics of Soft Hong Kong Marine Deposits without or with Cement Treatment.” *Lowland Technol. Int. 3*(1):1–13.

Yoshizaki, K., & Sakanoue, T., (2004), "Analytical Study on Soil-Pipeline Interaction Due to Large Ground Deformation," *13th World Conference on Earthquake Engineering, Vancouver, Canada*, Aug. 1–6, Paper No. 1402.

Zhang, Y. & Michalowski, R.L. (2015). "Thermal-Hydro-Mechanical Analysis of Frost Heave and Thaw Settlement." *Journal of Geotechnical and Geoenvironmental Engineering 141*(7):4015027.doi:10.1061/(ASCE)GT.1943-5606.0001305.